Next-to-leading order QCD predictions for $Z,\gamma^* + 3$-jet distributions at the Tevatron

C. F. Berger,[1] Z. Bern,[2] L. J. Dixon,[3] F. Febres Cordero,[4] D. Forde,[5,6] T. Gleisberg,[3] H. Ita,[2] D. A. Kosower,[7] and D. Maître[8]

[1]*Center for Theoretical Physics, MIT, Cambridge, Massachusetts 02139, USA*
[2]*Department of Physics and Astronomy, UCLA, Los Angeles, California 90095-1547, USA*
[3]*SLAC National Accelerator Laboratory, Stanford University, Stanford, California 94309, USA*
[4]*Departamento de Física, Universidad Simón Bolívar, Caracas 1080A, Venezuela*
[5]*Theory Division, Physics Department, CERN, CH-1211 Geneva 23, Switzerland*
[6]*NIKHEF Theory Group, Science Park 105, NL-1098 XG Amsterdam, The Netherlands*
[7]*Institut de Physique Théorique, CEA-Saclay, F-91191 Gif-sur-Yvette cedex, France*
[8]*Department of Physics, University of Durham, Durham DH1 3LE, United Kingdom*

(Received 23 April 2010; published 1 October 2010)

Using BLACKHAT in conjunction with SHERPA, we have computed next-to-leading order QCD predictions for a variety of distributions in $Z,\gamma^* + 1, 2, 3$-jet production at the Tevatron, where the Z boson or off-shell photon decays into an electron-positron pair. We find good agreement between the next-to-leading order results for jet p_T distributions and measurements by CDF and D0. We also present jet-production ratios, or probabilities of finding one additional jet. As a function of vector-boson p_T, the ratios have distinctive features which we describe in terms of a simple model capturing leading logarithms and phase-space and parton-distribution-function suppression.

DOI: 10.1103/PhysRevD.82.074002 PACS numbers: 12.38.−t, 12.38.Bx, 13.87.−a, 14.70.−e

I. INTRODUCTION

The Large Hadron Collider (LHC) recently passed the milestone of first collisions. The start of the LHC era in particle physics opens new opportunities to confront data with theoretical predictions for standard model scattering processes, at scales well beyond those probed in previous colliders. This confrontation will be a key tool in the search for new physics beyond the standard model. Where new physics produces sharp peaks, standard model backgrounds can be understood without much theoretical input. For many searches, however, the signals do not stand out so clearly, but are excesses in broader distributions of jets accompanying missing energy and charged leptons or photons. Such searches require a much finer theoretical understanding of the QCD backgrounds.

An important class of backgrounds is the production of multiple jets in association with a Z boson. If the Z boson decays into neutrinos, this process forms an irreducible background to LHC searches for new physics, such as supersymmetry, that are based on missing transverse energy and jets, as discussed in, e.g. Ref. [1]. These processes can be calibrated experimentally using events in which the Z boson decays into a pair of charged leptons, either an electron-positron pair or a dimuon pair. The latter samples are quite clean, and the QCD dynamics is of course identical to the $Z \to \nu\bar{\nu}$ mode. The one experimental drawback is the small branching ratio for $Z \to l^+l^-$. Nevertheless, there are already results from the Tevatron on Z production in association with up to three jets [2–5], along with the prospect of new analyses using larger data sets in the near future. Therefore in this paper we focus on the production of $Z + 1, 2, 3$ jets at the Tevatron, which can also serve as a benchmark for future LHC studies.

The first step toward theoretical control of QCD backgrounds at hadron colliders is the evaluation of the cross section at leading order (LO) in the strong coupling, α_S. Several computer codes [6–8] are available for LO predictions. These codes typically use matching (or merging) procedures [9,10] to incorporate higher-multiplicity leading-order matrix elements into programs that shower and hadronize partons [11–13]. Although such programs provide a hadron-level description which has great utility, the LO approximation suffers from large factorization- and renormalization-scale dependence, which grows with increasing jet multiplicity. This dependence is already up to a factor of 2 in the processes we shall study; accordingly, LO results do not generally provide a quantitatively reliable prediction. The problems go beyond that of normalization of cross sections: shapes of distributions may or may not be modeled correctly at (matched) LO, and the results at this order can depend strongly on the functional form and value chosen for the scale. In order to resolve these problems, and provide quantitatively reliable predictions, one must evaluate the next-to-leading order (NLO) corrections to processes of interest. Such computations are technically more challenging, but generically yield results with a greatly reduced scale dependence [14,15], as well as displaying better agreement with measurements (see e.g. Refs. [2,4,16,17]).

More generally, sufficiently accurate QCD predictions can provide important theoretical input into experimentally driven determinations of backgrounds, by allowing measurements in one process to be converted into a prediction for another, where theory is used only for the ratio of the two processes. For example, complete NLO predictions for $W + 3$-jet production, followed by $W \to l\nu$, are already

available at parton level [18], and the present paper describes analogous predictions for Z + 3-jet production, followed by $Z \to l^+ l^-$. These results allow the ratio of Z to W production in association with up to three jets to be computed at NLO. Parton-level results do neglect nonperturbative effects, such as hadronization and the underlying event, which can contribute to both Z and W production. However, as long as the experimental cuts on the jets are the same, the nonperturbative corrections should largely cancel in the Z to W ratio. Therefore, measurements of the (more copious) production of W bosons in the presence of multiple jets can be extrapolated to the case of Z bosons [19], using precise theoretical values for the ratio of Z to W events with similar kinematics, and as a function of the kinematics. Because leptonically decaying Z bosons, although rarer, are cleaner experimentally than W bosons, it has also been suggested to reverse the procedure and use $Z(\to l^+ l^-)$ boson samples to calibrate $W(\to l\nu)$ and $Z(\to \nu\bar{\nu})$ samples [20]. However, this procedure requires more input from theory: in order to have adequate statistics in the $Z \to l^+ l^-$ channel, less energetic kinematical configurations with larger cross sections are measured, and then extrapolated to more energetic configurations with smaller cross sections.

In the past, the bottleneck in computing NLO QCD corrections to processes with large numbers of jets has been the evaluation of one-loop amplitudes involving six or more partons [14]. On-shell methods [15,21–30] have successfully resolved this bottleneck, by avoiding gauge-noninvariant intermediate steps and reducing the problem to much smaller elements analogous to tree-level amplitudes. In this paper we evaluate the required one-loop amplitudes with the BLACKHAT program library [17,18,31,32], which implements on-shell methods numerically. A number of programs based on on-shell techniques have been constructed by other groups [33–37]. Approaches based on Feynman diagrams have also led to new results with six external partons, in particular, the NLO cross section for producing four heavy quarks at hadron colliders [38,39]. The $t\bar{t}b\bar{b}$ case has also been computed via on-shell methods [37], and recently the final state $t\bar{t}$ + 2 jets has been computed at NLO in a similar way [40]. We expect that on-shell methods will be especially advantageous for processes involving many external gluons, which often dominate multijet final states.

NLO parton-level cross sections for the production of a W or Z boson in association with one or two jets have long been available in the MCFM [41] code, which utilizes the one-loop amplitudes from Ref. [22] for the two-jet case. More recently, complete NLO results have been obtained for W + 3-jet production [18] using BLACKHAT in conjunction with the SHERPA package [13]. (Different leading-color approximations and ''adjustment procedures'' have also been applied to W + 3 jets at NLO [17,36].) In this work, we use the same basic calculational setup as in Ref. [18] to compute Z + 3-jet production. The real emission, dipole subtraction [42], and integration over phase space is handled by AMEGIC++ [8,43], which is part of the SHERPA package [13]. (Other automated implementations of infrared subtraction methods [42,44] have been described elsewhere [45].) SHERPA is also used to perform the Monte Carlo integration over phase space for all contributions. One important improvement in the present study with respect to Ref. [18] is to increase the efficiency of the phase-space integrator, making use of QCD antenna structures along the lines of Refs. [46,47].

In this article we present results for Z,γ^* + 3-jet production at the Tevatron to NLO in QCD, at parton level, and with the vector boson decaying to a lepton-antilepton pair. We include off-shell photon exchange, and $\gamma^* - Z$ interference, because the production of a charged-lepton pair by an off-shell photon is indistinguishable from the leptonic decay of a Z boson. Preliminary versions of some of the results presented here may be found in Ref. [48], where slightly different jet cuts were applied, along with a leading-color approximation.

Here we present total production cross sections, with jet and lepton cuts appropriate to existing CDF and D0 analyses [2,4], as well as a variety of distributions. We also study how Z,γ^* + 3-jet production at the Tevatron depends on a common choice of renormalization and factorization scale μ. As mentioned above, LO results are generically rather sensitive to the scale choice. This sensitivity usually is greatly reduced at NLO. As an example, in Z,γ^* + 3-jet production, varying the scale by a factor of 2 from our default central value causes nearly a 60% deviation from the central value. In contrast, at NLO this deviation drops to only 15%–22%.

Total cross sections with standard experimental jet cuts are dominated by the production of jets with low transverse momentum, $p_T < M_V$, where the vector boson V is a W or Z. Accordingly, scale choices such as the mass of the vector boson $\mu = M_V$ are reasonable for these quantities. For the study of differential distributions, however, it is better to choose a dynamical scale, event by event, in order to have reasonable scales for each bin [49]. This helps reduce the change in predicted shapes from LO to NLO, and can improve the NLO prediction some too. However, care is required in choosing the functional form of such scales. Greater care is required at the LHC than at the Tevatron, because the much larger dynamical range can ruin seemingly reasonable scale choices, such as the commonly used vector-boson transverse energy, $\mu = E_T^V \equiv \sqrt{M_V^2 + (p_T^V)^2}$ (see e.g. Refs. [2,4,16,17,50]). As noted in Ref. [18], a scale choice of $\mu = E_T^V$ leads to negative cross sections in tails of some NLO distributions, because typical energy scales in the process are much larger than E_T^V. In addition, as noted independently [51], the choice $\mu = E_T^V$ leads to undesirably large shape changes between LO and

NLO. As we discuss here, for Z + 3-jet production at the Tevatron, the scale $\mu = E_T^V$ is unsatisfactory, at least at LO: choosing it results in large shape changes in distributions between LO and NLO. The total partonic transverse energy $\hat{H}_T$ (or a fixed fraction thereof), adopted in our previous study [18], is a satisfactory choice. Other choices, such as the combined invariant mass of the jets [51], should also be satisfactory. In any case, the lesson is clear: the vector-boson transverse energy is not satisfactory and should not be used, especially for processes at the LHC.

At the Tevatron, both CDF and D0 have measured [2,4] jet-p_T distributions for Z,γ^* + 1, 2-jet production in the channel $Z \to e^+e^-$. The D0 measurements are not absolute cross sections, but are normalized to the inclusive Z, γ^* + 0-jet cross section for the same set of lepton cuts. CDF and D0 have each compared their data with NLO predictions from MCFM [41], taking into account estimates of nonperturbative corrections. For comparison we present our own NLO analysis of these processes. We then turn to the more involved case of Z, γ^* + 3-jet production, which we compare against the D0 experimental measurement. A difference between our NLO study and the experimental measurements is in our use of infrared-safe jet algorithms (as reviewed in Ref. [52]). Our default choice here is the SISCone jet algorithm [53], although we present some results using the anti-k_T algorithm [54] as well. (The k_T algorithm [55,56] gives parton-level results very similar to those for the anti-k_T one, so we do not present them.) The algorithms used in the CDF and D0 analyses, which are in the ''midpoint'' class of iterative cone algorithms [57–59], are generically infrared unsafe, and cannot be used in an NLO computation of V + 3-jet production. Although a midpoint algorithm will yield finite results at NLO for V + 2-jet production, it suffers from uncontrolled nonperturbative corrections that are in principle of the same order as the NLO correction [52].

In comparing theory and experiment, the differing jet algorithms do introduce an additional source of uncertainty. Nevertheless, based on our study of Z,γ^* + 1, 2-jet production we expect the NLO results to match experiment reasonably well. There have also been two studies comparing inclusive-jet cross sections for midpoint algorithms with those for SISCone [53,60], using PYTHIA [11], which find that the major nonperturbative differences between the algorithms are at the level of the underlying event. Although the kinematics of inclusive-jet production differs somewhat from that of a vector boson plus multiple jets, these results suggest that hadron-level data collected using SISCone would differ from that for midpoint algorithms primarily by the underlying-event correction (at least for larger cone sizes). That is, if the two measurements were corrected back to parton level, one would expect them to have only percent-level differences. (At the LHC, both ATLAS and CMS have adopted infrared-safe jet algorithms, removing this important source of uncertainty.)

We shall present Z,γ^* + 1, 2, 3-jet production cross sections for the CDF and D0 cuts, as well as jet p_T distributions. For Z,γ^* + 3-jet production, we show the p_T distributions for all three jets, ordered in p_T. In addition, we discuss ratios of cross sections. Experimental and theoretical systematic uncertainties cancel to some degree in such ratios. Ratios of similar processes—for example, the ratio of W + 3-jet to Z + 3-jet production—are thus attractive candidates for confronting experimental data with theoretical predictions. We shall not study this kind of ratio in the present paper, but another kind, that of a production process to the same process with one additional jet, sometimes known as the ''jet-production ratio'' [61,62]. (This ratio is also called the ''Berends'' or ''staircase'' ratio.) In particular, we study the ratio of Z,γ^* + n-jet to Z,γ^* + $(n-1)$-jet production up to $n = 4$ at LO and $n = 3$ at NLO. Its evaluation for different values of n can also test the lore, based on Tevatron studies, that the ratio is roughly independent of n. We find that for total cross sections through $n = 3$, with the experimental cuts used by CDF, this scaling is valid to about 30%, and for the D0 cuts, it is valid to about 15%.

One may also ask whether not just total cross sections, but also differential distributions, can be predicted for Z,γ^* + n-jet production (at least approximately) by scaling results for Z,γ^* + $(n-1)$-jet production. We show explicitly for $n \leq 4$, using the example of the vector-boson p_T distributions, that shapes of distributions *cannot* be reliably predicted by assuming a constant factor between the $(n-1)$-jet and n-jet cases. We describe the nontrivial structure found in the jet-production ratios for the vector-boson p_T distributions using a simple model that incorporates leading-logarithmic behavior and suppression due to phase-space and parton-distribution-function effects. Related to the shape differences is a strong dependence of the jet-production ratios on the experimental cuts. In particular, there is about a 50% difference in the jet-production ratios for the CDF and D0 setups, as shown in Tables VII and VIII of Sec. VI.

This paper is organized as follows. In Sec. II we briefly summarize our calculational setup, focusing on the differences from our previous work on W + 3-jet production [17,18]. Section III records our choice of couplings, renormalization and factorization scales, and cuts matching those of the CDF and D0 measurements. We also discuss issues associated with the choice of scale. In Sec. IV, we present results for cross sections and for a variety of distributions, matching CDF's cuts, and we compare with their measurements. In Sec. V we give distributions in the softest jet p_T for Z,γ^* + 1, 2, 3-jet production, using D0's cuts and comparing with their published data. In Sec. VI we present jet-production ratios for both the total cross section and the vector-boson p_T distribution, and discuss a simple model for the latter ratio. We present our conclusions in Sec. VII. We include one appendix

defining observables, as well as one giving values of the matrix elements at a single point in phase space. The latter appendix should aid future implementations of the $Z,\gamma^* + 3$-jet one-loop matrix elements.

II. CALCULATIONAL SETUP

A. Processes

In this paper we calculate the inclusive processes,

$$p\bar{p} \to Z, \gamma^* + n \text{ jets} + X \to e^+e^- + n \text{ jets} + X, \quad (2.1)$$

at $\sqrt{s} = 1.96$ TeV to NLO accuracy, for $n = 1, 2, 3$. Both CDF and D0 have measured production cross sections for all three of these processes [2,4] at the Tevatron, based on integrated luminosities of 1.7 fb^{-1} and 1.0 fb^{-1}, respectively. The D0 measurements, besides using slightly different cuts, use a significantly smaller jet cone size, $R = 0.5$ versus $R = 0.7$ for CDF. In addition, differential distributions have been provided for $Z,\gamma^* + 1$, 2-jet production. The set of available distributions is particularly extensive in the case of one jet [3,5]. The $Z,\gamma^* + 1$, 2-jet production measurements have been compared to NLO predictions from MCFM [41]. For the case of three additional jets, the data sets analyzed are still small, so that CDF has measured only a total cross section, while D0 has provided three bins in the distribution of the transverse momentum of the third jet (p_T ordered). The latter distribution was also compared with a leading-order prediction computed using MCFM.

The present article provides the first NLO predictions for $Z,\gamma^* + 3$-jet production, allowing a comparison with both the CDF cross section and the D0 p_T distribution. We will provide a few other distributions as well. We hope that, as additional data are analyzed, such distributions will be measured by CDF and D0. A comparison between NLO results and Tevatron data for various W, $Z + 3$-jet distributions would provide a very important benchmark for future LHC studies of these complex final states.

In more detail, the process under consideration (2.1) receives contributions from several partonic subprocesses. At leading order, and in the virtual (one-loop) NLO contributions, these subprocesses are all obtained from

$$q\bar{q}Q\bar{Q}g \to Z, \gamma^* \to e^+e^-, \quad (2.2)$$

$$q\bar{q}ggg \to Z, \gamma^* \to e^+e^-, \quad (2.3)$$

by crossing three of the partons into the final state. The quarks are represented by q and Q and the gluons by g. The Z or photon couples to the quark line labeled q. Representative diagrams for the virtual contributions are shown in Fig. 1. We include the decay of the vector boson (Z,γ^*) into a lepton pair at the amplitude level. The photon is always off shell, and the Z boson can be as well. For the Z the lepton-pair invariant mass, M_{ee}, follows a relativistic Breit-Wigner distribution whose width is determined by the Z decay rate Γ_Z. We take the lepton decay products to be massless. Amplitudes containing identical quarks are generated by antisymmetrizing in the exchange of appropriate q and Q labels.

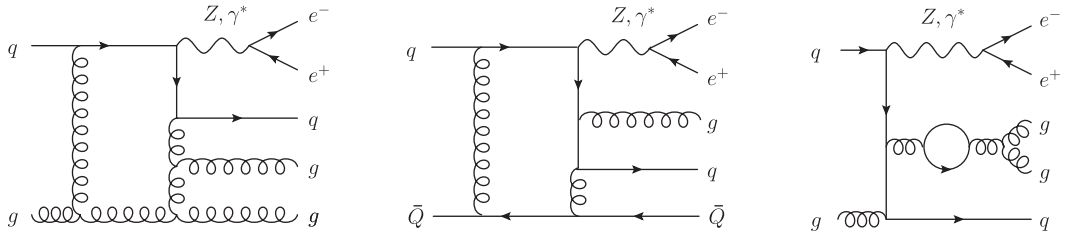

FIG. 1. A few representative diagrams contributing to the $qg \to e^+e^-qgg$ and $q\bar{Q} \to e^+e^-qg\bar{Q}$ one-loop amplitudes. The e^+e^- pair couples to the quarks via either a Z boson or an off-shell photon.

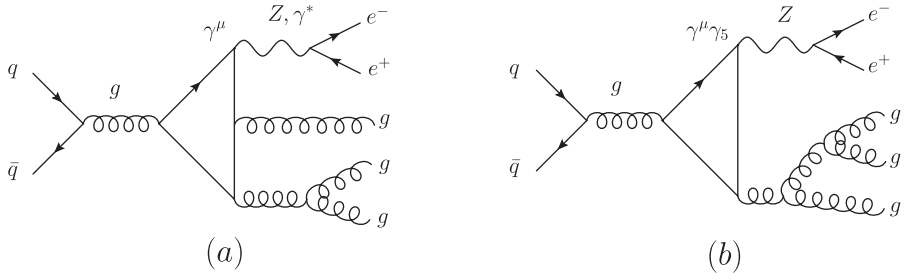

FIG. 2. Sample diagrams illustrating one-loop contributions to $Z,\gamma^* + 3$-jet production where the vector boson couples directly to a quark loop, via either (a) a vector coupling, or (b) an axial vector coupling. These contributions are quite small for the corresponding process with one parton less, and therefore are not included in our calculation.

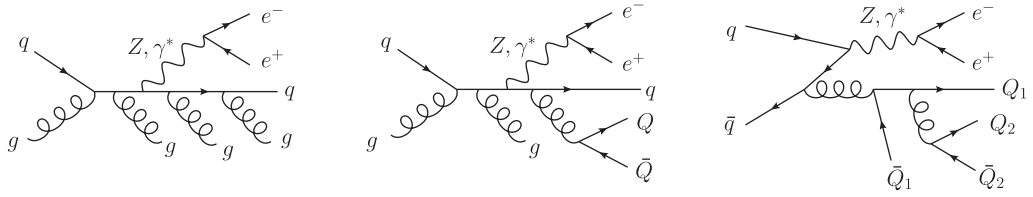

FIG. 3. Representative real-emission diagrams for the eight-point tree-level amplitudes, $qg \to e^+e^-qggg$, $qg \to e^+e^-qgQ\bar{Q}$, and $q\bar{q} \to e^+e^-Q_1\bar{Q}_1Q_2\bar{Q}_2$.

The light quarks, u, d, c, s, and b, are all treated as massless. We do not include contributions to the amplitudes from a real or virtual top quark. Nor do we include the pieces in which the vector boson couples directly to a quark loop through either a vector or axial coupling, as illustrated in Fig. 2. In $Z,\gamma^* + 2$-jet production these pieces affect the cross section by under 0.3%. We therefore expect the omission of these pieces to have a small effect on the $Z,\gamma^* + 3$-jet results presented here, well below the residual NLO uncertainties of 10%–20%.

Besides the loop amplitudes, we need tree amplitudes for real emission contributions. The relevant subprocesses are

$$q\bar{q}ggg \to Z, \gamma^* \to e^+e^-, \tag{2.4}$$

$$q\bar{q}Q\bar{Q}gg \to Z, \gamma^* \to e^+e^-, \tag{2.5}$$

$$q\bar{q}Q_1\bar{Q}_1Q_2\bar{Q}_2 \to Z, \gamma^* \to e^+e^-, \tag{2.6}$$

where all the physical processes are obtained by crossing four of the partons into the final state. Representative tree diagrams for these contributions are given in Fig. 3.

To compute the NLO corrections we use BLACKHAT and SHERPA, essentially following the same calculational setup described in Ref. [18] for the $W + 3$-jet process. We therefore discuss our setup only briefly, pointing out the few differences with Ref. [18].

B. Setup

The virtual contributions are evaluated with BLACKHAT, which is based on the unitarity method [21]. One-loop amplitudes are expanded in terms of a basis set of scalar integrals composed of box, triangle, and bubble integrals, plus a rational remainder. The coefficients of box integrals are obtained from quadruple cuts by solving the cut conditions [23]. Coefficients of bubble and triangle functions are then obtained using a numerical implementation of Forde's approach [27]. In this implementation, BLACKHAT uses a procedure related to that of Ossola, Papadopoulos, and Pittau [26] to subtract box contributions when determining triangle coefficients, and to subtract box and triangle contributions when determining bubble coefficients. The basis scalar integrals are evaluated numerically using their known analytic expressions [63]. To obtain rational terms, we have implemented both loop-level on-shell recursion [24,25] and a numerical version of the "massive continuation" approach due to Badger [64], which is related to the D-dimensional generalized unitarity [65] approach of Giele, Kunszt, and Melnikov [29]. The numerical version involves subtracting the contributions of higher-point cuts rather than taking large-mass limits. It is similar to the numerical version of Forde's method [27] for four-dimensional unitarity cuts, which is described in Ref. [18]. In that paper we used on-shell recursion for the leading-color terms, where speed is at a premium. For the simplest helicity configurations, on-shell recursion is implemented analytically and the results stored for numerical evaluation. For subleading-color terms the massive continuation method was used because it is presently more flexible. For production runs in the current study, we used the analytic formulas obtained via on-shell recursion for the leading-color amplitudes, and the massive continuation method for the remaining terms.

As discussed in Ref. [18], for efficiency purposes it is useful to compute the leading-color parts of the virtual contributions separately from the numerically much smaller, but computationally more complicated, subleading-color contributions. We follow the same division of leading and subleading color as in Ref. [18], except that here we assign the pieces proportional to the number of quark flavors (n_f) to the leading-color contributions instead of the subleading-color ones. This has the effect of somewhat reducing the size of the (already very small) subleading-color contributions, helping to reduce the number of phase-space points at which they must be evaluated. We add the leading- and subleading-color contributions at the end of the calculation to obtain the complete color-summed result. We refer the reader to Refs. [22,66] for detailed descriptions of the primitive amplitude decomposition that we used. Alternative organizations of color, within the context of the unitarity method, may be found in Refs. [34,67].

An important issue is the numerical stability of the loop amplitudes. In Fig. 4, we illustrate the stability of the full-color virtual interference term (or squared matrix element), $d\sigma_V$, summed over colors and over all helicity configurations for the two subprocesses $u\bar{u} \to e^+e^-u\bar{u}g$ and $u\bar{u} \to e^+e^-ggg$. The horizontal axis of Fig. 4 shows the logarithmic error,

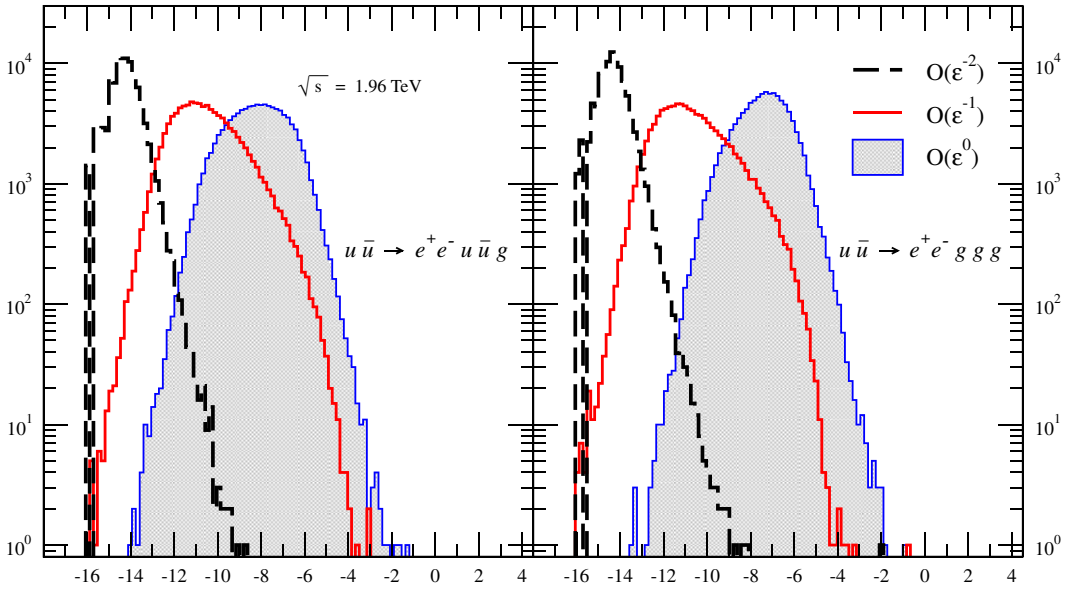

FIG. 4 (color online). The distribution of the relative error in the virtual cross section for the two subprocesses $u\bar{u} \to e^+e^-u\bar{u}g$ and $u\bar{u} \to e^+e^-ggg$. The horizontal axis is the logarithm of the relative error (2.7) between an evaluation by BLACKHAT, running in production mode, and a target expression evaluated using higher precision with at least 32 decimal digits (or up to 64 decimal digits for unstable points). The vertical axis shows the number of phase-space points out of 100 000 that have the corresponding error. The dashed (black) line shows the $1/\epsilon^2$ term; the solid (red) curve, the $1/\epsilon$ term; and the shaded (blue) curve, the finite (ϵ^0) term.

$$\log_{10}\left(\frac{|d\sigma_V^{\mathrm{BH}} - d\sigma_V^{\mathrm{target}}|}{|d\sigma_V^{\mathrm{target}}|}\right), \tag{2.7}$$

for each of the three components: $1/\epsilon^2$, $1/\epsilon$, and ϵ^0, where $\epsilon = (4 - D)/2$ is the dimensional regularization parameter. In this expression σ_V^{BH} is the cross section computed by BLACKHAT as it normally operates for production runs (switching from 16 decimal digits to higher precision only when instabilities are detected), whereas $\sigma_V^{\mathrm{target}}$ is a target value computed by BLACKHAT using multiprecision arithmetic with at least 32 digits, and 64 digits if the point is deemed unstable using the criteria described in Refs. [18,31]. We use the QD package [68] for higher-precision arithmetic. The phase-space points are selected in the same way as those used to compute cross sections. We note that an overwhelming majority (above 99.9%) of events are accurate to better than one part in 10^3—that is, to the left of the "-3" mark on the horizontal axis. Because we only need to recompute parts of amplitudes in most cases [18], the extra time spent in higher-precision operation is quite small, roughly 20% more than if only double precision had been used.

In addition to the virtual corrections, the real-emission corrections are also required. These terms arise from tree-level amplitudes with one additional parton: an additional gluon, or a quark-antiquark pair replacing a gluon, as illustrated in Fig. 3. We use SHERPA for these pieces. The infrared singularities are canceled between real-emission and virtual contributions using the Catani-Seymour dipole-subtraction method [42], implemented [43] in the automated program AMEGIC++ [8], which is part of the SHERPA framework [13]. We follow the same setup described in Ref. [18], taking $\alpha_{\mathrm{dipole}} = 0.03$ as our default value.

The Monte Carlo integration over phase space of both the real-emission and virtual pieces are carried out by SHERPA using a multichannel [69] approach. In this approach, the integrand is not split up into pieces, but is sampled differently in different channels. For $Z,\gamma^* + 1$, 2-jet production, we use AMEGIC++, and each channel generates a momentum configuration based on the size of the denominators of the propagators of a tree-level Feynman diagram (Born or real-emission, as appropriate). For the more complicated case of $Z,\gamma^* + 3$-jet production, in order to improve the efficiency, we have developed a specific phase-space generator, applicable to $V + n$-jet production. In this approach, a single channel generates a momentum configuration for the partons that is based on the size of denominators associated with a specific parton color ordering (the color-ordered QCD antenna radiation pattern), following the ideas of Refs. [46,47]. The lepton momenta are generated so that the invariant mass of the lepton pair traces a Breit-Wigner distribution about the vector-boson mass. For larger numbers of partons this generator has a greatly reduced number of channels, compared to the number of channels based on Feynman diagrams, so that it remains viable for vector-boson production with up to five or six jets.

For the $Z,\gamma^* + 3$-jet process we integrate the real-emission terms over about 4×10^7 phase-space points,

the leading-color virtual parts over 7×10^5 phase-space points, and the subleading-color virtual parts over 4×10^4 phase-space points. The LO and dipole-subtraction terms are run separately with 10^7 points each. These numbers are chosen to achieve an integration uncertainty of 0.5% or less in the total cross section.

As a cross-check, we have compared our results for $Z,\gamma^* + 0,1,2$-jet production at NLO and $Z,\gamma^* + 3$-jet production at LO to those of MCFM and find agreement to better than 1%. For $Z,\gamma^* + 2$-jet production we used the same analytic one-loop matrix elements [22] as used in MCFM, with cross-checks against a purely numerical computation within BLACKHAT.

III. COUPLINGS, EXPERIMENTAL CUTS, AND SCALE CHOICES

In this section we describe the basic parameters used in this work, including couplings, experimental cuts, and our choice of renormalization and factorization scales. We also discuss the residual scale dependence remaining in the NLO results.

A. Couplings and parton distributions

We express the Z-boson couplings to fermions using the standard model input parameters shown in Table I. The parameter g_w^2 is derived from the others via

$$g_w^2 = \frac{4\pi\alpha_{\rm QED}(M_Z)}{\sin^2\theta_W}. \tag{3.1}$$

We use the CTEQ6M [70] parton distribution functions (PDFs) at NLO and the CTEQ6L1 set at LO. The value of the strong coupling constant is fixed to agree with the CTEQ choices, so that $\alpha_S(M_Z) = 0.118$ and $\alpha_S(M_Z) = 0.130$ at NLO and LO, respectively. We evolve $\alpha_S(\mu)$ using the QCD beta function for five massless quark flavors for $\mu < m_t$, and six flavors for $\mu > m_t$. (The CTEQ6 PDFs use a five-flavor scheme for all $\mu > m_b$, but we use the SHERPA default of six-flavor running above the top-quark mass; the effect on the cross section is very small, on the order of 1% at larger scales.) At NLO we use two-loop running, and at LO, one-loop running.

TABLE I. Electroweak parameters used in this work.

Parameter	Value
$\alpha_{\rm QED}(M_Z)$	1/128.802
M_Z	91.1876 GeV
$\sin^2\theta_W$	0.230
Γ_Z	2.49 GeV

B. Experimental cuts for CDF

To compare to CDF data we apply the same cuts as CDF [2],

$$\begin{aligned} &p_T^{\rm jet} > 30\ {\rm GeV}, \qquad |y^{\rm jet}| < 2.1, \qquad E_T^e > 25\ {\rm GeV}, \\ &|\eta^{e_1}| < 1, \qquad |\eta^{e_2}| < 1 \quad \text{or} \quad 1.2 < |\eta^{e_2}| < 2.8, \\ &\Delta R_{e-{\rm jet}} > 0.7, \qquad 66\ {\rm GeV} < M_{ee} < 116\ {\rm GeV}. \end{aligned} \tag{3.2}$$

For any jet, $p_T^{\rm jet}$ denotes the transverse momentum and $y^{\rm jet}$ the rapidity. For the leptons, E_T^e denotes the transverse energy of either the electron or positron; η^{e_1} refers to the pseudorapidity of either the electron or positron, and η^{e_2} refers to that of the other; M_{ee} is the pair invariant mass.

In their study of Z,γ^* production, CDF used a midpoint jet algorithm [59] with a cone size of $R = 0.7$ and a merging/splitting fraction of $f = 0.75$. We use instead three different infrared-safe jet algorithms [53–55]: SISCone ($f = 0.75$), anti-k_T and k_T, all with $R = 0.7$. SISCone is our default choice for comparison to CDF. (The k_T algorithm gives very similar parton-level results as the anti-k_T algorithm, so we will not show those results explicitly.)

Our calculation is a parton-level one, and does not include corrections due to nonperturbative effects, such as those induced by the underlying event, induced, for example, by multiple parton interactions, or by fragmentation and hadronization of the outgoing partons. In order to compare our parton-level results to data, we require nonperturbative correction factors. As discussed further in Sec. IV B, for $Z,\gamma^* + 1$, 2-jet p_T distributions, we adopt estimates of these correction factors made by CDF [2].

C. Experimental cuts for D0

To compare to D0 data we apply the jet cuts [4],

$$p_T^{\rm jet} > 20\ {\rm GeV}, \qquad |\eta^{\rm jet}| < 2.5. \tag{3.3}$$

D0 defined jets using the D0 run II midpoint jet algorithm [58], with a cone size of $R = 0.5$ and a merging/splitting fraction of $f = 0.5$. We use instead the SISCone algorithm, with $R = 0.5$ and $f = 0.5$.

D0 performed an analysis with two distinct sets of lepton cuts. In their primary selection, which was compared directly to theory, only an invariant mass cut was imposed on the electron-positron pair,

$$\text{(a): } 65\ {\rm GeV} < M_{ee} < 115\ {\rm GeV}. \tag{3.4}$$

For the secondary selection, the lepton cuts were

$$\begin{aligned} \text{(b): } &65\ {\rm GeV} < M_{ee} < 115\ {\rm GeV}, \\ &E_T^e > 25\ {\rm GeV}, \\ &|\eta^e| < 1.1 \quad \text{or} \quad 1.5 < |\eta^e| < 2.5. \end{aligned} \tag{3.5}$$

The latter (b) selection corresponds to the data D0 actually collected. In their main selection [(a)], they extrapolated to an ideal detector with full lepton coverage using LO-matched parton-shower simulations. This extrapolation introduces an additional uncertainty and model dependence. It more than doubles the absolute cross section, although the quantities measured by D0, which are normalized by the inclusive $Z,\gamma^* + 0$-jet cross section for the same lepton cuts, shift by much less. [Comparing the (a) entry to the corresponding (b) entry in Table IV gives an estimate of the fraction of cross section in selection (a) that comes from the extrapolation.]

We shall present NLO results corresponding to both selections, that is with and without the lepton acceptance cuts in the secondary selection (3.5). Selection (b) allows us to compare to unextrapolated data. On the other hand, D0 estimated the nonperturbative corrections, from hadronization and the underlying event, for selection (a) [4], requiring us to extrapolate these corrections to selection (b) in order to use them there, as we shall discuss further in Sec. V.

D. Scale dependence

Following the standard procedure, we test the stability of the perturbative results by varying the renormalization and factorization scales. In this article, we set the renormalization and factorization scales equal, $\mu_R = \mu_F = \mu$. In Figs. 5 and 6, we show the scale variation of the total cross section for the SISCone and anti-k_T algorithms, respectively. In both cases we choose the central scale $\mu_0 = M_Z$ and then vary it down by a factor of 4 and upwards by a factor of 8. A fixed scale of the order of the Z mass is appropriate here, because the cross section is dominated by low-p_T jets. In both figures, the upper three panels show the markedly reduced scale dependence at NLO compared to the corresponding LO cross section in $Z,\gamma^* + 1$-, $Z,\gamma^* + 2$-, and $Z,\gamma^* + 3$-jet production, respectively. The bottom panel combines the ratios of NLO to LO predictions (K factors) for all three cases, illustrating the increasing sensitivity of the LO result with an increasing number of jets. This increase is expected, because there is an additional power of α_s for every additional jet. Accordingly, the reduction in the scale dependence at

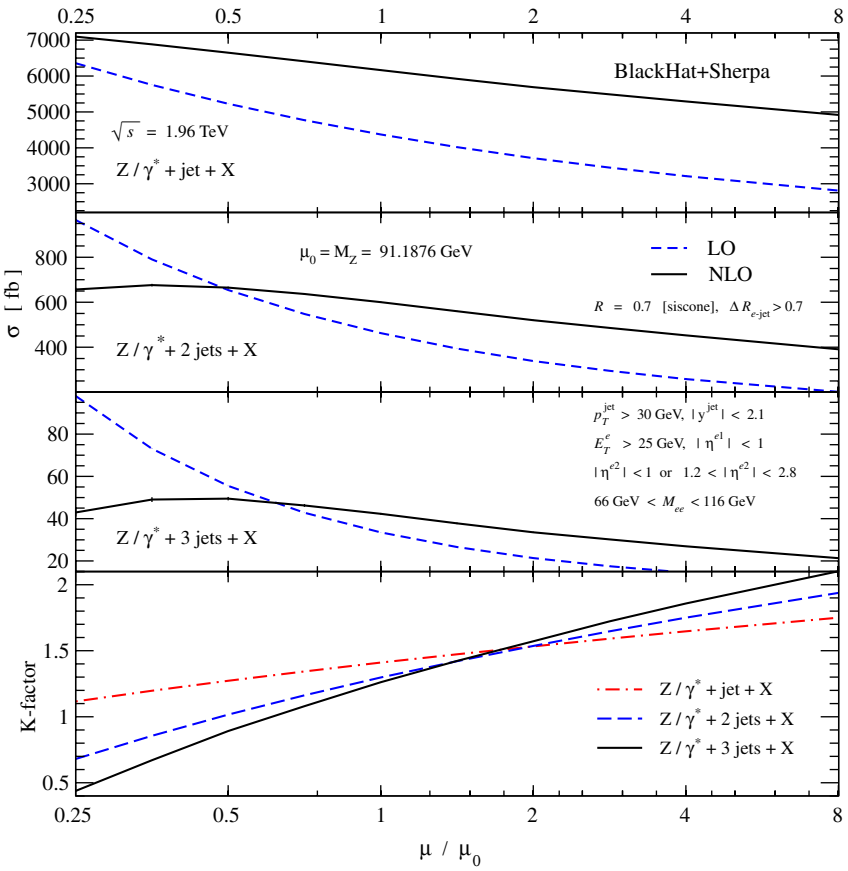

FIG. 5 (color online). The scale dependence of the LO (dashed blue lines) and NLO (solid black lines) cross sections for Z, $\gamma^* + 1$, 2, 3-jet production at the Tevatron, as a function of the common renormalization and factorization scale μ, with $\mu_0 = M_Z$. Here the SISCone jet algorithm is used; the lepton and jet cuts match CDF [2]. The bottom panels show the K factor, or ratio between the NLO and LO result, for each of the three cases: 1 jet (dot-dashed red line), 2 jets (dashed blue lines), and 3 jets (solid black lines).

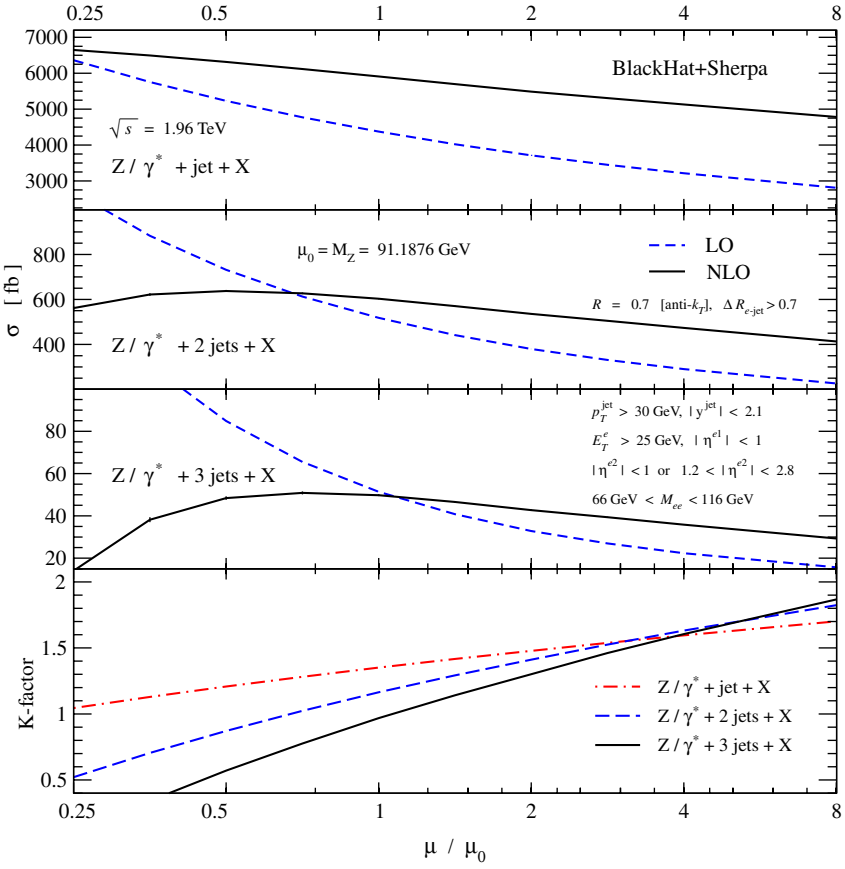

FIG. 6 (color online). The scale dependence for $Z,\gamma^* + 1, 2, 3$-jet production at the Tevatron. The plot is the same as Fig. 6, except here the anti-k_T jet algorithm is used.

NLO tends to become more significant with an increasing number of jets. The plots for the k_T algorithm are very similar to the ones for anti-k_T, so we do not show them here.

Figures 5 and 6 also reveal two further features. First, for $n > 1$ the cross section for the anti-k_T algorithm is significantly larger than for SISCone at the same value of R, especially at LO; the difference lessens at NLO. Second, the K factor at $\mu = M_Z$ decreases significantly with the number of jets. The first feature is due to the smaller probability of two partons clustering into a jet in the anti-k_T algorithm. In that algorithm (or in the k_T algorithm), no clustering can take place unless the two partons are separated by less than R in the (η, ϕ) plane; whereas in SISCone they can be clustered out to a distance of $2R$. Hence the effective radius of a cone algorithm, for the same value of R, is somewhat larger (by a factor of about 1.35) than that of a cluster algorithm such as anti-k_T or k_T [52,56,71]. At LO, clustering always causes a loss of events, and thus a decreased cross section for SISCone, relative to anti-k_T. NLO corrections, however, tend to increase the cross section more for jet algorithms with larger effective cone areas, because there is less chance of radiating a parton out of the cone and thereby reducing the jet p_T below the cut threshold [52,71]. Hence the cross-section difference between the algorithms is lessened at NLO. The differences between SISCone and k_T algorithms at LO and NLO can also be examined as a function of the number of jets in $W + 1, 2, 3$-jet production, using results for the LHC presented in Ref. [18]. However, in this work $R = 0.4$ was used, resulting in far smaller perturbative differences between the algorithms.

The second feature, in which the K factors at $\mu = M_Z$ decrease with the number of jets, is not unrelated. It was previously observed that $W + 3$-jet production for $R = 0.4$ had quite a small K factor [17,18,36]. The dependence on the number of jets was discussed in Ref. [72], where it was attributed to the LO cross section being "too high," in part because of collinear enhancements associated with the small jet size. We can see from Figs. 5 and 6 that the trend of the decreasing K factor is stronger for the anti-k_T algorithm than for SISCone. This feature is consistent with the picture of Ref. [72], because the anti-k_T algorithm effectively has a smaller jet size.

For distributions, rather than total cross sections, we would like to choose a characteristic renormalization and factorization scale on an event-by-event basis, in particular, to ensure that the tails of distributions are described

properly. Previous studies (see e.g. Refs. [2,4,16,17,50]) have used the transverse energy of the vector boson, E_T^V, as a common renormalization and factorization scale. As already argued in Refs. [18,51] this choice is quite poor at LHC energies. Indeed, because of the large dynamic range at the LHC, at NLO the choice can go disastrously wrong for some distributions, leading to negative cross sections [18]. It also causes large changes in shapes of generic distributions between LO and NLO. This behavior reflects the emergence of large logarithms $\ln\mu/E$, which spoil the validity of the perturbative expansion when μ does not match the characteristic energy scale E. We note that without an NLO result for guidance, it may not be clear that a given scale choice—such as E_T^V—is problematic.

Even for the Tevatron, with its smaller dynamic range, the commonly used scale choice $\mu = E_T^V$ is not particularly good. It leads to a large change in shape between LO and NLO in the p_T distribution of the third-hardest jet in Z, γ^* + 3-jet production, as shown in the left panel of Fig. 7. In contrast, the scale choice $\mu = \hat{H}_T/2$, where $\hat{H}_T$ is the total partonic transverse energy defined in Eq. (A4), results in little change in shape between LO and NLO. This choice is shown in the right panel of Fig. 7.

The difficulty with using the vector-boson transverse energy, $\mu = E_T^Z$, as the scale can be exposed [18] by considering the two configurations depicted in Fig. 8. In configuration (a), the Z boson has a transverse energy larger than that of the jets, and sets the scale for the process. In configuration (b), the two leading jets roughly balance in p_T, while the Z has much lower transverse energy. Here, the scale $\mu = E_T^Z$ is too low, and not characteristic of the process. In the tails of Fig. 7, configuration (b) dominates, because it results in a larger third-jet p_T for fixed center-of-mass partonic energy; contributions from higher center-of-mass energies which might boost the Z-boson transverse energy are suppressed by the falloff of the parton distributions. This explains the large deviation between LO and NLO visible in the left panel of Fig. 7.

In contrast, $\hat{H}_T$ (or some fixed fraction of it) does properly capture both configurations (a) and (b). It is thus a much better choice of scale. [For the purposes of fixing the scale, we prefer the partonic definition of the total transverse energy over the experimental one in Eq. (A5) because it is independent of the experimental cuts and the jet definitions [18].] In the remainder of this paper we take $\mu = \hat{H}_T/2$ as our default for both the renormalization and factorization scales, except where noted. To assess the remaining scale dependence in the cross sections we evaluate them at five scales: $\mu/2$, $\mu/\sqrt{2}$, μ, $\sqrt{2}\mu$, and 2μ. We generate scale variation bands using the minimum and maximum values. In our previous analysis [18] of W production in association with jets at the LHC, we chose $\mu = \hat{H}_T$. Generally, $\hat{H}_T$ tends to be on the high side of typical energy scales, so here we divide by a factor of 2. The difference between the two choices at NLO is not

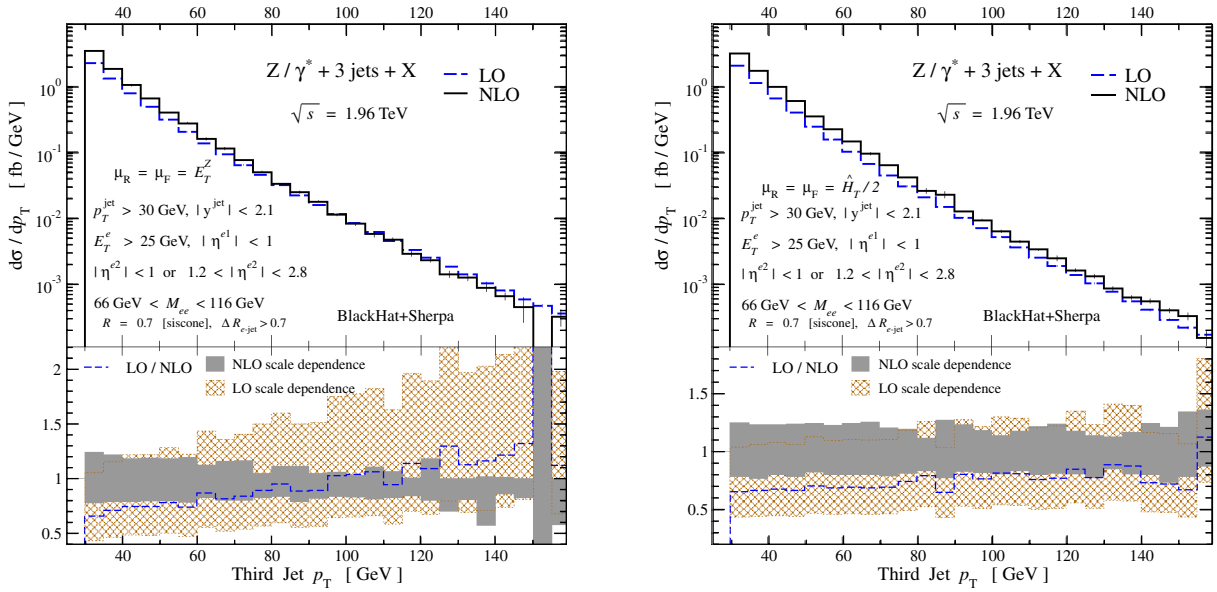

FIG. 7 (color online). The NLO p_T distribution of the third jet in Z, γ^* + 3-jet production at the Tevatron, for the SISCone algorithm. In the left panel the scale choice $\mu = E_T^Z$ is used and for the right panel $\mu = \hat{H}_T/2$. The thin vertical lines (where visible) indicate the numerical integration uncertainties. The bottom part of each panel displays various ratios, where the denominator is always the NLO result at the reference scale choice, and the numerator is obtained by either evaluating the LO result at the same scale (dashed blue line), varying the LO scale by a factor of 2 in either direction (cross-hatched brown band), or varying the NLO scale in the same way (gray band). Although the two NLO results are compatible, the LO results have large shape differences, illustrating why $\mu = E_T^Z$ is not a good choice at LO. The jet and lepton cuts match those used by CDF [2].

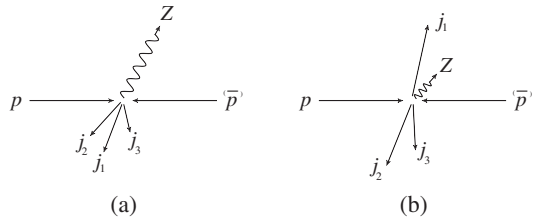

FIG. 8. Two distinct $Z + 3$ jet configurations with rather different values for the Z transverse energy. In (a) an energetic Z balances the energy of the jets, while in (b) the Z is relatively soft. (b) generally dominates over (a) when the transverse energy of the third jet gets large.

large, on the order of 10% in the normalization, and with very small effects on the shapes of distributions. At LO the changes are, of course, larger, with up to 40% variations.

Although we adopt here $\mu = \hat{H}_T/2$ as a good representative overall scale for general distributions, other approaches may be superior for particular distributions, or particular regions of phase space. For example, it may be possible to resum large logarithms that appear in particular corners of phase space, and match the resummed result to the NLO one. Even if that cannot be done, it is certainly possible that choosing a scale that is a blend of different scales (such as the different jet transverse momenta) is appropriate in some cases.

In principle, perturbative approximations can break down in various kinematic regions, so it is important to check whether this can affect our results. The breakdown is often due to effects of soft-gluon emission that can be resummed in many cases. Large soft-gluon effects can be obtained when there are explicit vetoes on soft radiation, or when such radiation is implicitly vetoed by fast-falling parton distribution functions. In this paper, we put no explicit vetoes on soft radiation in any observable we consider. However, there is an implicit veto as one goes out in the tail of the H_T distribution or the third-jet p_T distribution. This implicit veto might lead to large double Sudakov, or threshold, logarithms.

In order to investigate whether such logarithms might be large, we take advantage of the fact that threshold logarithms in the high-p_T tail of the p_T distribution for inclusive jet production should be very similar to the tails we are looking at in $V + n$-jet production, at comparable values of jet p_T. In both cases there is a comparable mix of partonic channels, and similar values of parton x. Note, however, that one can reach much higher p_T's experimentally in pure jet production because of the much larger cross sections. One recent resummation of threshold logarithms for inclusive jet production [73] shows that the effects are quite modest. For example, Fig. 6 of Ref. [73] shows the ratio K of the (matched) next-to-leading logarithmic (NLL) result to the NLO result for single-inclusive jet production at the Tevatron run I ($\sqrt{s} = 1.8$ TeV), for p_T from 50 to 500 GeV. For various choices of the renormalization and factorization scales, K ranges from 0.98 to at most 1.14, as long as $p_T < 300$ GeV. Note that 300 GeV is well above the third-jet p_T's shown in Fig. 7. (The relevant parton x values probed at the Tevatron in Fig. 6 of Ref. [73] also correspond at the LHC to p_T's that are about 7 times larger, well above the range studied in Fig. 9 of Ref. [18]. There, the NLO cross section evaluated at $\mu = E_T^V$ became negative for a second-jet E_T of only 475 GeV. Hence, even in this more extreme example, threshold logarithms are very unlikely to play a role in this behavior.)

There is one other type of logarithm in $V + n$-jet production, which is not present in inclusive jet production, and that is a (double) logarithm of the form $\ln(p_{T,\mathrm{jet}}/M_V)$, due to emission of electroweak vector bosons that are soft and collinear with respect to the jets, as in the configuration shown in Fig. 8(b). The importance of this logarithm was emphasized very recently [74] for the case of $Z + 1$-jet production. Although the NLO correction to this process is enhanced by $\alpha_s \ln^2(p_{T,\mathrm{jet}}/M_V)$ with respect to LO, the effect is peculiar to $V + 1$-jet production. It does not happen when two or more final-state partons are present at LO, because then the configuration in Fig. 8(b) can already be reached at LO. Also, because it is associated with *electroweak* boson emission, it does not represent a *QCD* double logarithm that will reappear at higher orders in α_s.

We conclude that there is no indication of a breakdown of fixed-order perturbation theory for the ranges of observables studied in this paper or in Ref. [18].

IV. RESULTS FOR CDF

In this section we present results for $Z,\gamma^* + 1$, 2, 3-jet production (inclusive) at the Tevatron, and compare to data from CDF that has been corrected back to the hadron level [2]. For jet p_T distributions in $Z,\gamma^* + 1$, 2-jet production, we use the (relatively large) nonperturbative corrections estimated by CDF [2] to transform our parton-level results to hadron-level ones. For $Z,\gamma^* + 3$-jet production, nonperturbative corrections were not explicitly presented by CDF, and we give only parton-level results.

A. Total cross sections

In Table II we present the total inclusive cross sections for $Z,\gamma^* + 1$, 2, 3-jet production, showing both the CDF measurement and theoretical predictions, using our default scale choice $\mu = \hat{H}_T/2$. The theoretical results in the table are given for both the SISCone and anti-k_T jet algorithms. (The k_T algorithm gives identical results as the anti-k_T algorithm at LO, and is within 1% at NLO.) In the second column we give the CDF measurement, for its midpoint jet algorithm and corrected to hadron level, along with the experimental uncertainties. The statistical, systematic (upper and lower) and luminosity uncertainties are given after the central values. The third and fourth columns present the LO and NLO parton-level predictions. Here

TABLE II. $Z,\gamma^* + 1, 2, 3$-jet production (inclusive) cross section (in fb) at CDF. The column labeled CDF gives the hadron-level results from Ref. [2], using a midpoint jet algorithm. The experimental uncertainties are statistical, systematics (upper and lower), and luminosity. The columns labeled by LO parton and NLO parton contain the parton-level results for the SISCone and anti-k_T jet algorithms. The central scale choice for the theoretical prediction is $\mu = \hat{H}_T/2$, the numerical integration uncertainty is in parentheses, and the scale dependence is quoted in super- and subscripts. Nonperturbative corrections should be accounted for prior to comparing the CDF measurement to parton-level NLO theory.

No. of jets	CDF midpoint	LO parton SISCone	NLO parton SISCone	LO parton anti-k_T	NLO parton anti-k_T
1	$7003 \pm 146^{+483}_{-470} \pm 406$	$4635(2)^{+928}_{-715}$	$6080(12)^{+354}_{-402}$	$4635(2)^{+928}_{-715}$	$5783(12)^{+257}_{-334}$
2	$695 \pm 37^{+59}_{-60} \pm 40$	$429.8(0.3)^{+171.7}_{-111.4}$	$564(2)^{+59}_{-70}$	$481.2(0.4)^{+191}_{-124}$	$567(2)^{+31}_{-57}$
3	$60 \pm 11^{+8}_{-8} \pm 3.5$	$24.6(0.03)^{+14.5}_{-8.2}$	$36.8(0.2)^{+8.8}_{-7.8}$	$37.88(0.04)^{+22.2}_{-12.6}$	$44.7(0.24)^{+5.1}_{-6.8}$

TABLE III. $Z,\gamma^* + 1, 2, 3$-jet production cross section (in fb) at CDF. This table is similar to Table II, except that here the scale choice is $\mu = E_T^Z$.

No. of jets	CDF midpoint	LO parton SISCone	NLO parton SISCone	LO parton anti-k_T	NLO parton anti-k_T
1	$7003 \pm 146^{+483}_{-470} \pm 406$	$4206(2)^{+801}_{-616}$	$6076(9)^{+501}_{-466}$	$4206(2)^{+801}_{-616}$	$5828(9)^{+425}_{-414}$
2	$695 \pm 37^{+59}_{-60} \pm 40$	$422.2(0.3)^{+168}_{-109}$	$576(2)^{+72}_{-77}$	$469.4(0.4)^{+185}_{-120}$	$583(2)^{+51}_{-67}$
3	$60 \pm 11^{+8}_{-8} \pm 3.5$	$28.66(0.03)^{+17.9}_{-10.0}$	$40.3(0.2)^{+8.6}_{-8.5}$	$43.28(0.05)^{+26.6}_{-14.9}$	$48.7(0.3)^{+3.8}_{-7.9}$

we quote the uncertainties from integration statistics in parentheses, and the scale dependence in super- and subscripts (upper and lower). The scale dependence is determined following the traditional prescription of varying the scale by a factor of 2 around the central choice $\mu = \hat{H}_T/2$, as described above.

To assess the effect of changing the jet algorithm, we compare the SISCone and anti-k_T results in Table II, which further quantifies the differences that were visible in Figs. 5 and 6, which used a fixed scale μ. Although the SISCone algorithm gives noticeably different results from the anti-k_T algorithm, the variations are similar in magnitude

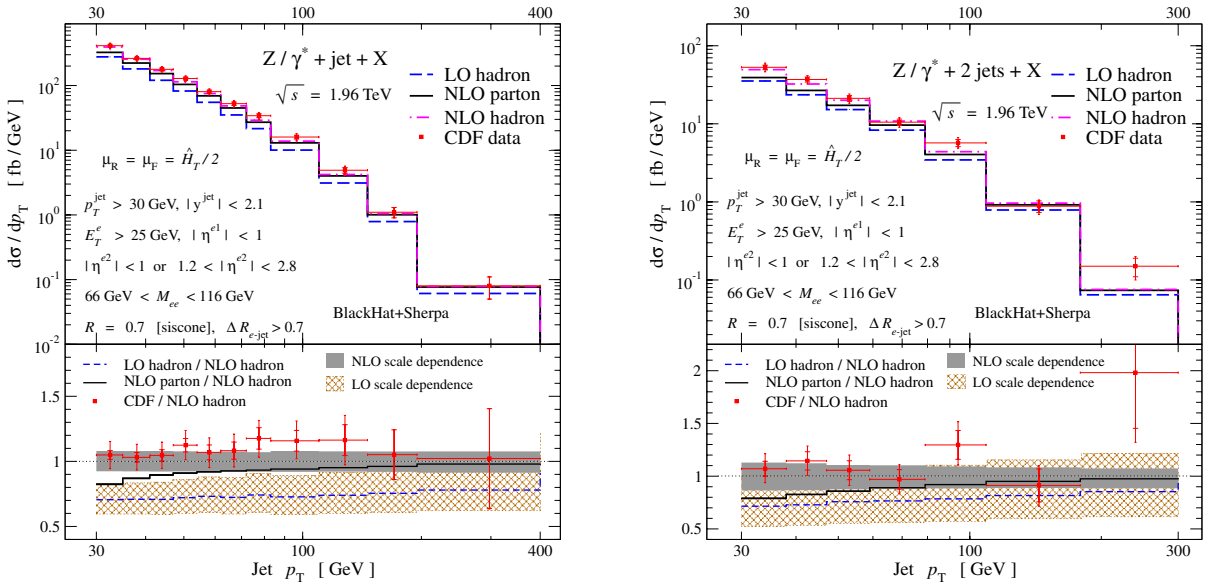

FIG. 9 (color online). Jet p_T distributions for $Z,\gamma^* + 1, 2$-jet production at the Tevatron with CDF's cuts. The theoretical predictions use the SISCone algorithm and the scale choice $\mu = \hat{H}_T/2$. In the upper panels the parton-level NLO distribution are the solid (black) histograms, and the NLO distributions corrected to hadron level are given by dash-dotted (magenta) curves. The CDF data are the (red) points, whose inner and outer error bars denote, respectively, the statistical and total uncertainties on the measurements (the latter obtained by adding separate uncertainties in quadrature). The LO predictions have been corrected to hadron level and are shown as dashed (blue) lines. The lower panels show the distributions normalized to the full hadron-level NLO prediction for $\mu = \hat{H}_T/2$. The scale-dependence bands in the lower panels are shaded (gray) for the NLO prediction corrected to hadron level and cross-hatched (brown) for LO corrected to hadron level.

to the residual scale dependence. The reasons for the perturbative differences between SISCone and anti-k_T algorithms were outlined in Sec. III D.

It is also interesting to compare the results of Table II to cross sections obtained with the widely used scale $\mu = E_T^Z$ instead of our default choice $\mu = \hat{H}_T/2$. In Table III we give cross sections with this scale choice for the SISCone and anti-k_T jet algorithms. Comparing these results to those of Table II, we see that, at least for $Z,\gamma^* + 1$, 2 jets, the K factor (ratio of NLO to LO) is much closer to unity for the choice $\mu = \hat{H}_T/2$, than for $\mu = E_T^Z$. Although the $\mu = E_T^Z$ choice is problematic in general, as already noted in Sec. III, at NLO it gives results for the total cross section that are similar to those from our default choice of $\mu = \hat{H}_T/2$.

In order to compare parton-level results to the experimental measurement we must account for nonperturbative corrections, using estimates from CDF [2]. These corrections are sizable, increasing the total cross section by a factor between 1.1 and 1.4 as the number of jets increases from one to three. As we will see in Fig. 9 for the jet p_T distributions, these estimated correction factors align NLO theory with the measurement within uncertainties, although a much more careful study of the nonperturbative corrections and the differences in jet algorithms is needed. It is interesting to note that in the CDF measurement of $W + n$-jet production [16], the corrections are significantly smaller. That measurement used a jet cone size of $R = 0.4$ (with the JETCLU algorithm [75]). There the hadronization and underlying-event corrections were under 10% below 50 GeV and under 5% at higher E_T. The CDF study may also be contrasted with the D0 study [4] discussed below, in which the cone size of $R = 0.5$ leads to nonperturbative corrections on the order of 15%. From the perspective of maintaining the precision of NLO predictions, it is advantageous to choose jet-cone sizes which minimize nonperturbative corrections, while not increasing the size of ($\ln R$-enhanced) higher-order perturbative corrections too much. As discussed in e.g. Refs. [52,71], there is a tradeoff between the underlying-event correction (increases as R increases) and splashout (increases as R decreases), and a careful study would be needed to find the best choice.

B. Comparison to CDF jet p_T distributions

In this section, we compare our results with CDF data for jet p_T distributions in $Z,\gamma^* + 1$-jet and $Z,\gamma^* + 2$-jet production. In the observables used by CDF, sometimes referred to as inclusive-jet p_T distributions, all jets passing the cuts are included in the distributions. That is, if n jets pass the cuts, the event is counted n times, with contributions to each of the n bins containing the transverse energy of one of the jets. By definition, for inclusive $Z + n$-jet production, at least n jets pass the cuts, and periodically additional jets can also pass the cuts. At NLO these extra jets are modeled by a single extra jet from the real-emission contribution. This causes the area under the curve to be slightly more than n times the total cross section. In contrast, the $W + n$-jet production distributions measured in Ref. [16] and the $Z + n$-jet production distributions measured in Ref. [4] are differential in the transverse energy (or momentum) of the nth jet, and each event is counted only once, so they integrate to give the total cross section for $V + n$-jet production.

The left and right panels of Fig. 9 are for $Z,\gamma^* + 1$-jet and $Z,\gamma^* + 2$-jet production, respectively. The upper part of each panel compares the LO and NLO results against CDF data from Ref. [2]. BLACKHAT + SHERPA produces NLO parton-level predictions. To compare to the CDF measurement we need to account for nonperturbative corrections. We use the last column of Table I of Ref. [2] as an estimate of their size. This table of corrections was determined for the CDF midpoint jet algorithm using PYTHIA [11], an LO-based parton-shower, hadronization and underlying-event program. Because we used the (infrared-safe) SISCone algorithm, the possible algorithm dependence of the nonperturbative corrections introduces additional uncertainty into the comparison. As mentioned in the Introduction, studies [53,60] of inclusive-jet cross-section differences between midpoint algorithms and SISCone (which were also performed for $R = 0.7$) suggest relatively small "parton-level" differences between the algorithms, which in turn suggest that applying the CDF nonperturbative corrections to our SISCone perturbative prediction is not unreasonable. The size of the corrections can be seen in the upper panels of Fig. 9 by comparing the curves labeled "NLO parton," which are the parton-level predictions, to the ones labeled "NLO hadron," which are the hadron-level ones. It is easier to judge the size in the lower panels, using the solid (black) curves which give the ratios of the two predictions. For example, for $Z,\gamma^* + 2$-jet production, nonperturbative corrections are significant for low p_T, on the order of 20% at 30 GeV, and gradually drop to under 5% at larger jet transverse momenta. Uncertainties in the nonperturbative corrections are not included in the plots.

The bottom panels shows various ratios, normalized to the NLO hadron-level prediction for the central scale $\mu = \hat{H}_T/2$. We include scale-dependence bands, as described above, for the predictions corrected to hadron level. As expected, for NLO the scale dependence is greatly reduced when compared to LO. We note that for both $Z,\gamma^* + 1$, 2-jet production, the NLO hadron-level jet p_T distributions match the CDF results quite well, noticeably better than the hadron-level LO distributions or parton-level NLO distributions. A similar comparison of the experimental data to NLO predictions was given in the CDF study, using MCFM [41]. The ratios of data to NLO presented there differ by up to 10% from those shown in Fig. 9. Most of the difference can be attributed to the choice of central scale in the NLO result, $\mu = E_T^Z$ versus $\mu = \hat{H}_T/2$. CDF also assessed the

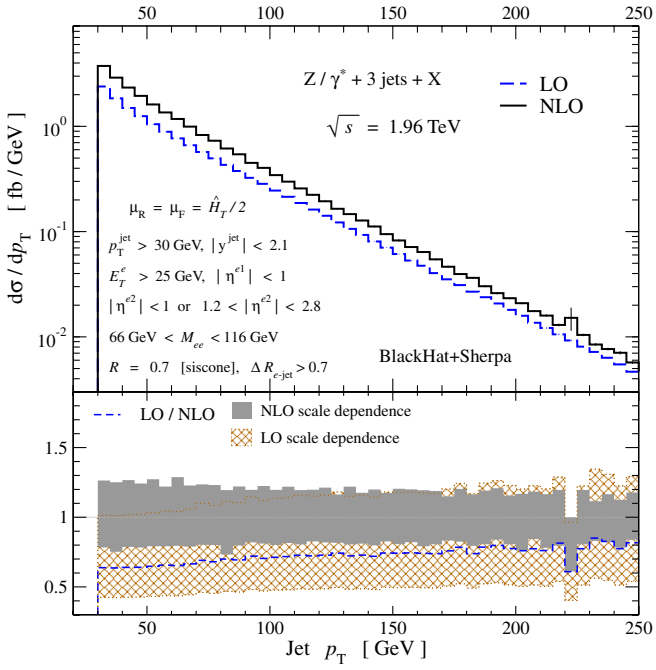

FIG. 10 (color online). p_T of all jets for $Z,\gamma^* + 3$-jet production with the CDF setup, using the SISCone jet algorithm and the scale choice $\mu = \hat{H}_T/2$, for LO and NLO at parton level. The thin vertical lines (where visible) indicate the numerical integration uncertainties. The lower panel bands are normalized to the central NLO prediction, as in Fig. 9.

uncertainties on the NLO predictions arising from the parton distribution functions. They found them to vary from 4% at low jet p_T to 10% at high p_T, which is generally smaller than the NLO scale variation.

C. Predictions for $Z,\gamma^* + 3$-jet distributions at CDF

In Fig. 10, we show the combined distribution of all jet p_T's in $Z,\gamma^* + 3$-jet production. It would be very interesting to compare this prediction to CDF data, after accounting for nonperturbative effects. As discussed above, the integral under the curve gives a bit more than 3 times the total cross section. As can be seen in the plot, with the scale choice $\mu = \hat{H}_T/2$ there is only a modest change in shape between LO and NLO, especially at higher jet p_T. This is similar to the parton-level results for $Z,\gamma^* + 1, 2$-jet production shown in Fig. 9. We expect nonperturbative corrections to lead to larger shape changes at lower p_T.

The separate distributions for the hardest, second-hardest, and third-hardest jet are shown in Fig. 11. The shapes of the LO and NLO distributions are again similar, with our default scale choice. As in $W + 3$-jet production [18], successive jets have increasingly steeply falling distributions.

In Fig. 12 we show the η distribution of the positron for $Z,\gamma^* + 1, 2, 3$-jet production. The discontinuity and gap between $\eta = \pm 1$ and $\eta = \pm 1.2$ result from the discontinuity in the charged-lepton cuts in Eq. (3.2). A careful

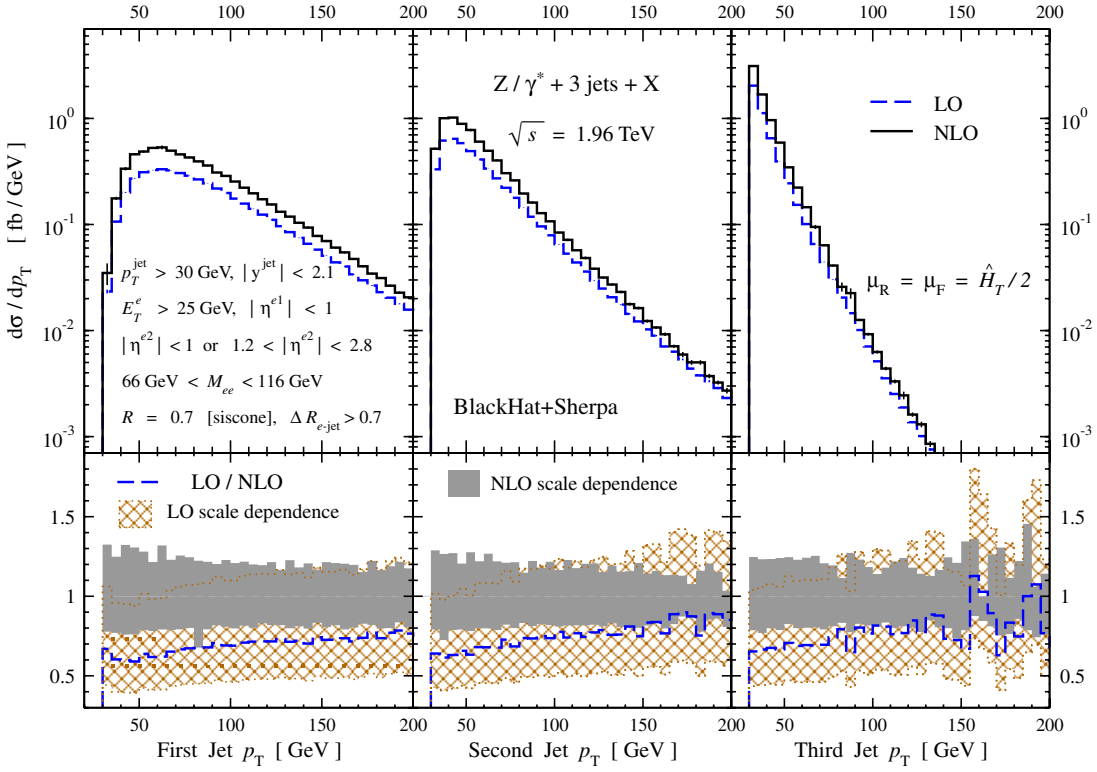

FIG. 11 (color online). First, second, and third jet p_T distributions for $Z,\gamma^* + 3$-jet production. The dashed (blue) lines are LO predictions and the solid (black) lines are NLO predictions. The SISCone jet algorithm and a scale choice of $\mu = \hat{H}_T/2$ are used for these plots.

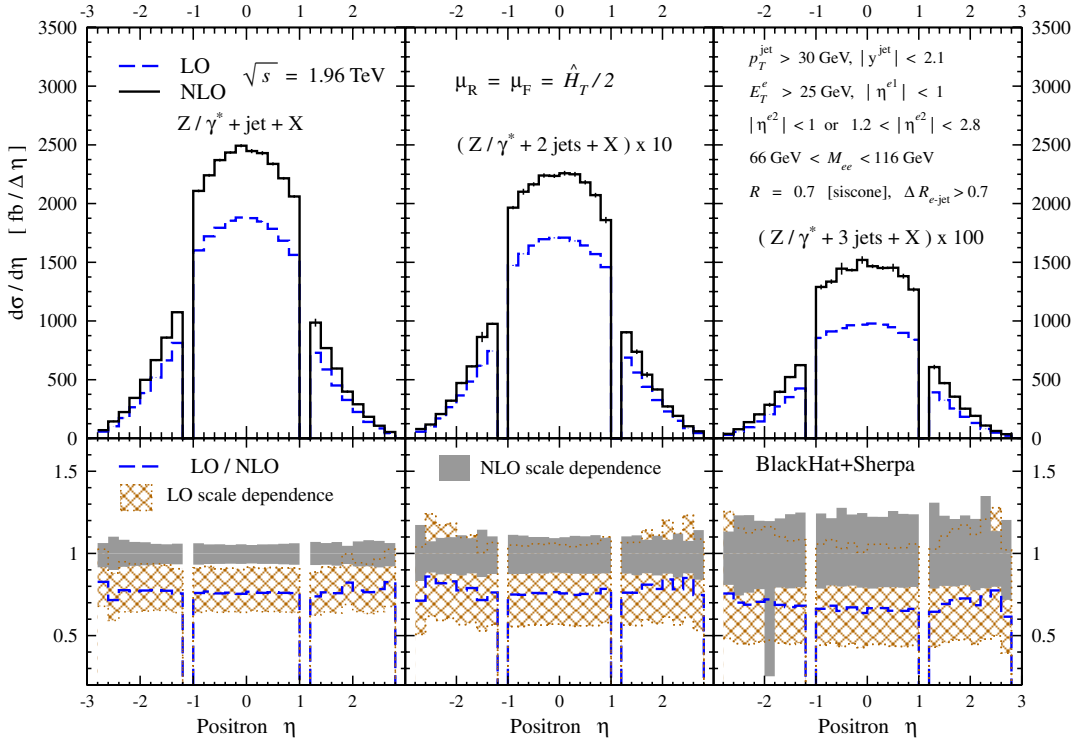

FIG. 12 (color online). The η distribution of the positron, for $Z,\gamma^* + 1, 2, 3$-jet production. The discontinuities in the plots are due to the experimental cuts (3.2). The cross sections in the second and third panels are multiplied by factors of 10 and 100, respectively.

inspection reveals a small forward-backward asymmetry, which can be traced to the left-right asymmetry in the Z boson couplings to fermions. (Similar asymmetries are discussed in e.g. Ref. [76].) Once again, there is only a modest shape change between LO and NLO.

V. RESULTS FOR D0

The D0 Collaboration has studied jet p_T distributions in inclusive $Z,\gamma^* + n$-jet production for up to three jets [4], using the D0 run II midpoint jet algorithm. Here we present the corresponding NLO parton-level results. To compare NLO theory and experiment we again need to account for nonperturbative corrections. D0 has provided estimates of nonperturbative corrections due to the underlying-event and hadronization effects for their study using the lepton cuts (a) of Eq. (3.4). With the smaller cone size used by D0, $R = 0.5$, the net nonperturbative corrections turn out to be no larger than about 15%, significantly smaller than in the CDF analysis for $R = 0.7$. As described further below, we will use these correction factors as a rough estimate of the nonperturbative corrections for selection (b) as well.

A. Total cross section

The theoretical predictions for the total cross sections for selection (a), with lepton cuts (3.4), and for selection (b), with lepton cuts (3.5), are given in Table IV. The LO and NLO parton-level cross sections are for the SISCone algorithm, with the central scale choice $\mu = \hat{H}_T/2$, and the scale dependence determined as before. For the case of $Z,\gamma^* + 0$-jet production we use $\mu = E_T^Z$, because $\mu = \hat{H}_T/2$ can vanish. As seen from Table IV, for $Z,\gamma^* + 1, 2, 3$-jet production the LO scale dependence is quite large, but is substantially reduced at NLO. In particular, for $Z,\gamma^* + 3$-jet production a shift in

TABLE IV. NLO parton-level $Z,\gamma^* + 0, 1, 2, 3$-jet production cross sections corresponding to D0 selections (a) and (b). The columns labeled by LO parton and NLO parton correspond to the parton-level results for the SISCone algorithm. The central scale used for one or more jets is $\mu = \hat{H}_T/2$. The numerical integration uncertainties are in parentheses and the scale dependence in super- and subscripts.

No. of jets	LO parton selection (a)	NLO parton selection (a)	LO parton selection (b)	NLO parton selection (b)
0 (pb)	$179.01(0.02)^{+0.}_{-0.649}$	$236.96(0.08)^{+3.75}_{-2.48}$	$84.08(0.03)^{+0.78}_{-0.64}$	$106.81(0.15)^{+0.88}_{-0.40}$
1 (fb)	$25\,223(9)^{+5011}_{-3877}$	$30\,230(55)^{+1212}_{-1667}$	$10\,083(6)^{+1927}_{-1501}$	$12\,537(44)^{+580}_{-721}$
2 (fb)	$3787(3)^{+1539}_{-999}$	$4415(14)^{+260}_{-476}$	$1538(2)^{+608}_{-398}$	$1848(10)^{+127}_{-201}$
3 (fb)	$462.3(0.5)^{+280}_{-158}$	$553(3)^{+70}_{-92}$	$190.2(0.2)^{+113}_{-64}$	$236(1)^{+30}_{-42}$

the scale by a factor of 2 causes a variation of up to 60% at LO and under 20% at NLO. For the case of $Z,\gamma^* + 0$-jet production, the scale dependence of the LO result is anomalously small [77]. This scale independence is due to the absence of factors of the strong coupling α_s in the LO matrix elements, along with the mild dependence of the quark distribution functions $q(x, \mu_F)$ on μ_F at values of x that are relevant at the Tevatron.[1]

In Ref. [4], D0 provided jet p_T distributions rather than summed cross sections. We could, of course, use the differential measurement to obtain the total cross section for $Z,\gamma^* + 1, 2, 3$-jet production (as a fraction of the inclusive Z-boson production cross section), but as the systematic error correlations were not specified, we instead turn to a direct comparison of theory and experiment for the p_T distributions.

B. Comparison to D0 jet p_T distributions

We now compare our predictions for jet p_T distributions to the D0 measurements. From our vantage point, selection (a) allows a direct comparison of our NLO predictions to the plots presented in Ref. [4], which also include results from various LO and parton-shower based programs. On the other hand, as noted earlier, in selection (a) more than half the events are extrapolated from the actual measurement using the cuts (3.5) of selection (b). This extrapolation introduces additional uncertainty into the measurement. Thus selection (b) would normally be preferred for comparison to theory. However, because the nonperturbative corrections determined in Ref. [4] were for selection (a), they do not directly apply to selection (b). Selection (b) corresponds to a subset of (a), which could have somewhat different average values for the Z-boson rapidity and transverse momenta; these values could in turn affect the jet kinematics and therefore the nonperturbative corrections. Because the correlation between lepton cuts and jet kinematics is at second order, and because the quoted nonperturbative corrections for (a) are no larger than about 15%, one may hope that the corrections for (b) are not too different. For either selection, we face the same issue as with CDF, that the nonperturbative corrections were estimated for a midpoint jet algorithm rather than SISCone. In light of these issues, we present NLO parton-level results with the SISCone algorithm as our primary predictions. We then adopt the nonperturbative corrections given in Ref. [4] for both selections (a) and (b), leaving possible (significant) improvements to future studies.

In the comparison, we follow D0 in normalizing the $Z,\gamma^* + 1, 2, 3$-jet p_T distributions by dividing by the inclusive $Z,\gamma^* + 0$-jet cross section. The latter cross section is defined using the same set of lepton cuts as applied in the numerator, for both the (a) and (b) selections. When assessing the scale dependence, we vary the scale by a factor of 2 in each direction in the numerator, but in the denominator for simplicity we always take the central-scale values in the first row of Table IV. Because both the LO and NLO inclusive Z,γ^* cross sections vary by under 2% from their central values, this procedure modifies the scale variation band only slightly, with respect to varying scales in the denominator as well.

We have compared D0 data for $Z,\gamma^* + 1, 2, 3$-jet production to our NLO prediction for both selections (a) and (b). Reference [4] already showed a comparison between selection (a) for inclusive $Z,\gamma^* + 1, 2$-jet production and NLO predictions using MCFM [41], so for these processes, we show instead a comparison to selection (b). The comparison is displayed in Fig. 13. As explained above, we use Tables IV and V of Ref. [4] to convert our parton-level results to hadron-level ones. Reference [4] studied the effects of parton distribution function uncertainties on the perturbative predictions for selection (a), and found them to be 5%–10% for the leading two jets, and 5%–15% for the third jet. We have compared our results for both selections (a) and (b) to MCFM, using the k_T algorithm with scale choice $\mu = E_T^Z$; we find agreement, with the total cross section agreeing to better than 0.5%. [As was the case for the CDF study, the ratio of data to NLO presented by D0 differs by up to 10% from our corresponding results, though for selection (b), in Fig. 13; again the difference is largely due to the different choice of central scale in the NLO result, $\mu = E_T^Z$ versus $\mu = \hat{H}_T/2$.]

Figure 14 compares our theoretical predictions for the third-jet p_T distribution in $Z,\gamma^* + 3$-jet production to both selections (a) and (b). As expected, the scale dependence of the NLO predictions is quite a bit smaller than for LO, throughout the distribution, with only a 15% deviation from the central value. For reference, we also present the results shown in Fig. 14 in tabular form, in Tables V and VI. The columns labeled ''LO parton'' and ''NLO parton'' give the parton-level results. These are the primary results of our D0 study, and would be the key input to any future analyses. The columns labeled ''LO/NLO hadron'' give these predictions multiplied by the nonperturbative corrections given in Table VI of Ref. [4] and represent a rough estimate. As in Fig. 14 we have not included the uncertainties in the nonperturbative corrections. Finally, the column labeled ''D0'' gives the D0 measurement, followed by its statistical and systematic uncertainties. Figure 14 and Tables V and VI show that, although the experimental central values are always a bit above the theoretical bands, the agreement between theory and experiment is reasonable, given the experimental statistical uncertainties, and despite the various unquantified uncertainties discussed above. For both theory and experiment, the shift in values

[1]The smaller scale variation of inclusive Z,γ^* production at LO, with respect to NLO, does not, of course, imply that the LO prediction is more accurate; indeed, the NLO result is much closer to the NNLO one [77].

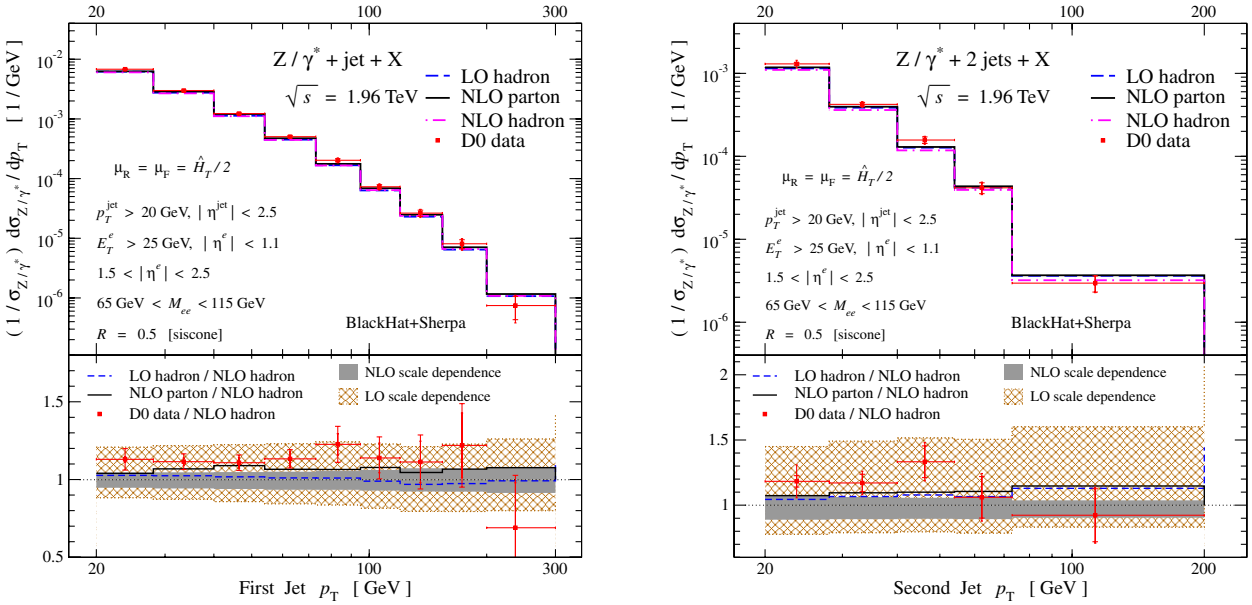

FIG. 13 (color online). Normalized jet p_T distributions for D0 selection (b). The left plot shows $1/\sigma_{Z,\gamma^*} \times d\sigma/dp_T$ for the leading jet in $Z,\gamma^* + 1$-jet production. The right plot shows the distribution for the second-hardest jet in $Z,\gamma^* + 2$-jet production. The SISCone algorithm and scale choice $\mu = \hat{H}_T/2$ are used in the theoretical predictions. In the upper panels the parton-level NLO distributions are the solid (black) histograms, while the NLO distributions corrected to hadron level are given by dash-dotted (magenta) histograms. The D0 data are indicated by the (red) points; the inner and outer error bars denote, respectively, the statistical and total experimental uncertainties on the measurements. The LO predictions corrected to hadron level are shown as dashed (blue) lines. Each lower panel shows the distribution normalized to the full hadron-level NLO prediction. The scale-dependence bands in the lower panels are shaded (gray) for NLO and cross-hatched (brown) for LO.

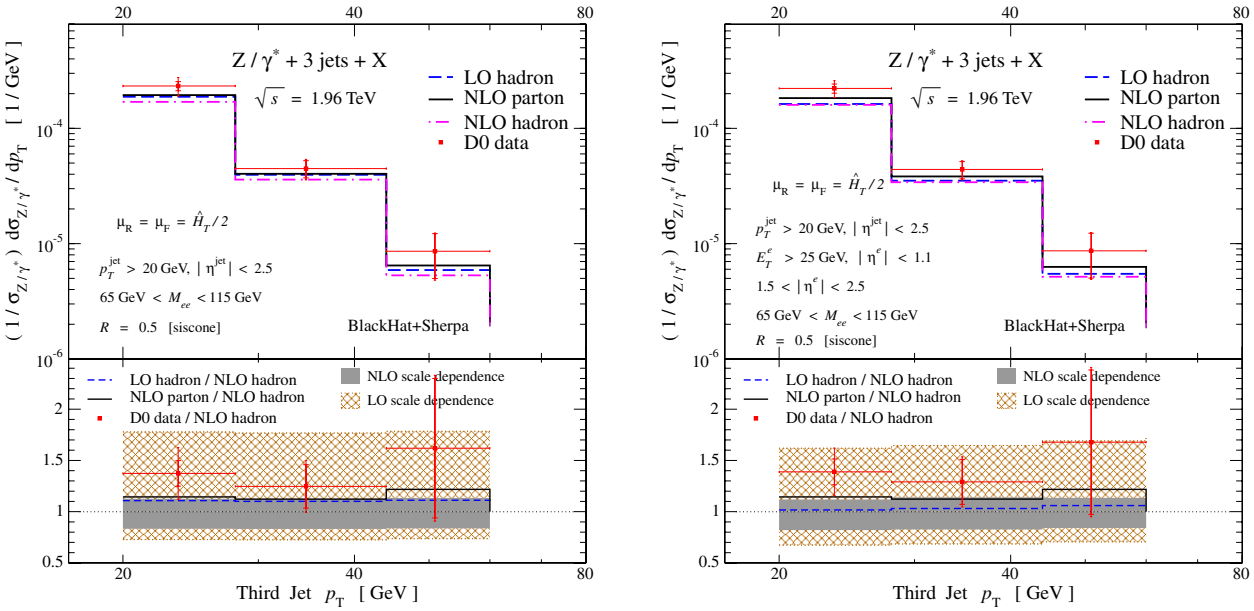

FIG. 14 (color online). Comparison of NLO theory to the D0 result for the distribution of $1/\sigma_{Z,\gamma^*} \times d\sigma/dp_T$ for the third-hardest jet in inclusive $Z,\gamma^* + 3$-jet production. The left plot shows the comparison for selection (a), and the right plot for selection (b). The quoted [4] nonperturbative corrections for (a) were used as estimated for both selections. The SISCone jet algorithm and the scale $\mu = \hat{H}_T/2$ were used in the theoretical predictions. The labeling is as in Fig. 13.

TABLE V. $Z,\gamma^* + 3$-jet production for D0 selection (a), $1/\sigma_{Z,\gamma^*} \times d\sigma/dp_T$ for the third jet (p_T ordered) in inclusive $Z, \gamma^* + 3$-jet production, with the lepton cuts of Eq. (3.4). The LO and NLO hadron columns include hadronization and underlying-event corrections from Ref. [4]. The hadron-level columns do not include the uncertainties from nonperturbative corrections; estimates of these may be found in Table VI of Ref. [4].

p_T bin (GeV)	LO parton (10^{-6}/GeV)	NLO parton (10^{-6}/GeV)	LO hadron (10^{-6}/GeV)	NLO hadron (10^{-6}/GeV)	D0 (10^{-6}/GeV)
20–28	$215(0.3)^{+130}_{-74}$	$194(1.5)^{+25}_{-32}$	$188(0.4)^{+114}_{-65}$	$170(1.3)^{+22}_{-28}$	$233 \pm 21 \pm 37$
28–44	$44.4(0.06)^{+26.9}_{-15.1}$	$40.3(0.2)^{+5.0}_{-1.1}$	$39.5(0.05)^{+24.0}_{-13.5}$	$35.9(0.2)^{+4.3}_{-0.9}$	$44.8 \pm 7.6 \pm 4.9$
44–60	$7.19(0.02)^{+4.35}_{-2.43}$	$6.47(0.09)^{+0.86}_{-0.11}$	$5.90(0.01)^{+3.57}_{-1.99}$	$5.31(0.08)^{+0.71}_{-0.86}$	$8.60 \pm 3.61 \pm 1.12$

TABLE VI. $Z,\gamma^* + 3$-jet production. $1/\sigma_{Z,\gamma^*} \times d\sigma/dp_T$ for the third jet (p_T ordered) in inclusive $Z,\gamma^* + 3$-jet production. The setup is the same as in Table V, except the additional lepton cuts given in Eq. (3.5) for selection (b) are imposed. In the columns labeled by "hadron" we again multiplied by the nonperturbative corrections [computed for (a)] from Table VI of Ref. [4].

p_T bin (GeV)	LO parton (10^{-6}/GeV)	NLO parton (10^{-6}/GeV)	LO hadron (10^{-6}/GeV)	NLO hadron (10^{-6}/GeV)	D0 (10^{-6}/GeV)
20–28	$186(0.3)^{+23}_{-63}$	$183(1.3)^{+22}_{-32}$	$162(0.3)^{+21}_{-55}$	$160(1.1)^{+19}_{-29}$	$222 \pm 20 \pm 31$
28–44	$39.4(0.07)^{+23}_{-13}$	$38.3(0.3)^{+5.5}_{-6.7}$	$35.2(0.07)^{+20.9}_{-11.8}$	$34.1(0.3)^{+6.6}_{-5.9}$	$44.0 \pm 7.5 \pm 3.7$
44–60	$6.66(0.02)^{+3.97}_{-2.23}$	$6.29(0.09)^{+0.85}_{-1.00}$	$5.47(0.02)^{+3.26}_{-1.83}$	$5.17(0.08)^{+0.70}_{-0.82}$	$8.67 \pm 3.64 \pm 0.95$

between selections (a) and (b) is quite small, significantly smaller than the respective uncertainties.

VI. JET-PRODUCTION RATIOS

The measurement of jet cross sections is sensitive to a number of experimental and nonperturbative issues, in particular the measurement of the jet energy and contributions due to the underlying event. The latter is not modeled in perturbative predictions, and accordingly introduces a systematic uncertainty. Jet p_T distributions fall rapidly: the distribution of the third-hardest jet in $Z + 3$-jet production in Fig. 11, for example, falls by 2 orders of magnitude over a factor-of-2 range in p_T. Thus small errors in p_T measurements or nonperturbative shifts in jet p_T can have important effects on distributions. Furthermore, the cross section for an additional jet is roughly an order of magnitude smaller, so a misidentification of an $(n-1)$-jet process as an n-jet process can cause a significant error in the measured cross section for the process with the extra jet. These difficulties increase as the number of jets accompanying a vector boson grows.

A simple way to control some of the systematic uncertainties is to consider instead ratios of cross sections [61,62,78]. As an example, consider the jet-production ratio (also known as the Berends or staircase ratio), the ratio of $Z,\gamma^* + n$-jet to $Z,\gamma^* + (n-1)$-jet production, displayed in Table VII for the CDF cuts (3.2) and in Table VIII for D0 type (b) cuts (3.5). We expect such ratios to be much less sensitive to experimental systematic measurement uncertainties than the individual cross sections.[2] Ratios also mitigate various theoretical uncertainties, such as uncertainties in the nonperturbative corrections. The theoretical values in Tables VII and VIII are given at parton level. In assessing the scale dependence of the ratio, we varied the renormalization and factorization scales (by a factor of 2) in the same way for both numerator and denominator. (Of course, one could consider alternative schemes to estimate scale dependence.) Lacking knowledge of the correlations between the experimental systematic uncertainties, we took them to be uncorrelated. (We also took the larger of the upper and lower uncertainties, as they are quite close for all cases.) Both the NLO and LO results are compatible with the experimental ratios, within the estimated uncertainties. It would be interesting to reexamine these ratios using the larger data set collected more recently at the Tevatron, and properly incorporating all correlations in the experimental systematic uncertainties.

Previous studies have noted that the jet-production ratios are roughly independent of the base number of jets. With the choice of cuts used by CDF, Eq. (3.2), our NLO

TABLE VII. The ratios of the $Z,\gamma^* + n$-jet to $Z,\gamma^* + (n-1)$-jet cross sections for CDF's cuts, using the SISCone algorithm and $\mu = \hat{H}_T/2$. For the experimental uncertainties we removed the luminosity errors, as these cancel; we treated all remaining uncertainties as uncorrelated. For the theoretical ratios we varied the scale in the same way in the numerator and the denominator. The integration uncertainties are small compared to the remaining scale dependence.

Jet ratio	CDF	LO	NLO
2/1	0.099 ± 0.012	$0.093^{+0.015}_{-0.012}$	$0.093^{+0.004}_{-0.006}$
3/2	0.086 ± 0.021	$0.057^{+0.008}_{-0.006}$	$0.065^{+0.008}_{-0.007}$
4/3	...	$0.040^{+0.005}_{-0.004}$	...

[2]Note that the jet-energy scale uncertainty will not completely cancel, however, because the p_T distribution in the nth jet is steeper than that in the $(n-1)$st jet.

TABLE VIII. The ratios of the $Z,\gamma^* + n$-jet to $Z,\gamma^* + (n-1)$-jet cross sections for D0's selection (b), using the SISCone algorithm and $\mu = \hat{H}_T/2$. Here we keep only the experimental statistical uncertainties and drop the systematic ones. The scale dependence is treated as in the previous table.

Jet ratio	D0	LO	NLO
2/1	0.151 ± 0.005	$0.153^{+0.026}_{-0.020}$	$0.147^{+0.003}_{-0.008}$
3/2	0.139 ± 0.012	$0.124^{+0.018}_{-0.013}$	$0.128^{+0.007}_{-0.010}$
4/3	⋯	$0.104^{+0.013}_{-0.010}$	⋯

theoretical results for $n = 2, 3$ are similar, within 30% of each other. With D0's choice of cuts, the agreement is better, to within 15%. The predicted ratio for $n = 4$ is significantly lower, but this prediction is still only at LO, because the NLO results for $Z,\gamma^* + 4$-jet production are not yet available. Tables VII and VIII also show that the NLO predictions for the jet-production ratios are quite close to the LO central values, but tend to have less scale variation.

This approximate independence, however, hides a great deal of variation in differential distributions. In Fig. 15, we show the differential distributions in the vector-boson transverse momentum (p_T^V) for inclusive $Z,\gamma^* + 1, 2, 3, 4$-jet production at LO (left panel) and for inclusive $Z,\gamma^* + 1, 2, 3$-jet production at NLO (right panel). The lower panes show the corresponding ratios: $(Z, \gamma^* + 2\text{-jet})/(Z, \gamma^* + 1\text{-jet})$ (2/1), $(Z, \gamma^* + 3\text{-jet})/(Z, \gamma^* + 2\text{-jet})$ (3/2), $(Z, \gamma^* + 4\text{-jet})/(Z, \gamma^* + 3\text{-jet})$ (4/3) at LO; 2/1 and 3/2 at NLO. These ratios have shapes that are quite stable in going from LO to NLO, as shown in Fig. 16, with the exception of the 2/1-jet ratio at low p_T and small differences in the 3/2 ratio at higher p_T. In these plots, we use parton-level results, without any corrections for hadronization or the underlying event. We expect substantial cancellations of these nonperturbative corrections in the ratios.

This figure shows that the jet-production ratios depend strongly on the p_T of the vector boson, and that the 3/2-jet and 2/1-jet ratios are rather different beyond low p_T. This means that their putative independence of the base number of jets is illusory: in reality, they depend sensitively on the cuts applied. For example, a $p_T > 70$ GeV cut on the vector-boson transverse momentum would result in a rather sizable difference between the 3/2-jet and 2/1-jet ratios of total cross sections.

How does the nontrivial dependence of these ratios on p_T^V arise? At LO, the 2/1-jet ratio is undefined (infinite) at low p_T^V; it rises smoothly from a very small value at $p_T^V = p_{T\,\mathrm{min}}^{\mathrm{jet}}$, where $p_{T\,\mathrm{min}}^{\mathrm{jet}}$ is the minimum jet p_T set by the experimental cut (30 GeV in this case). In contrast, at NLO the 2/1-jet ratio rises to a finite value as $p_T^V \to 0$. The other ratios have no structure at low p_T. All of the ratios rise noticeably beyond p_T^V of 70 GeV or so, a rise which continues up to around 200 GeV, where the ratios flatten out or start to decline somewhat.

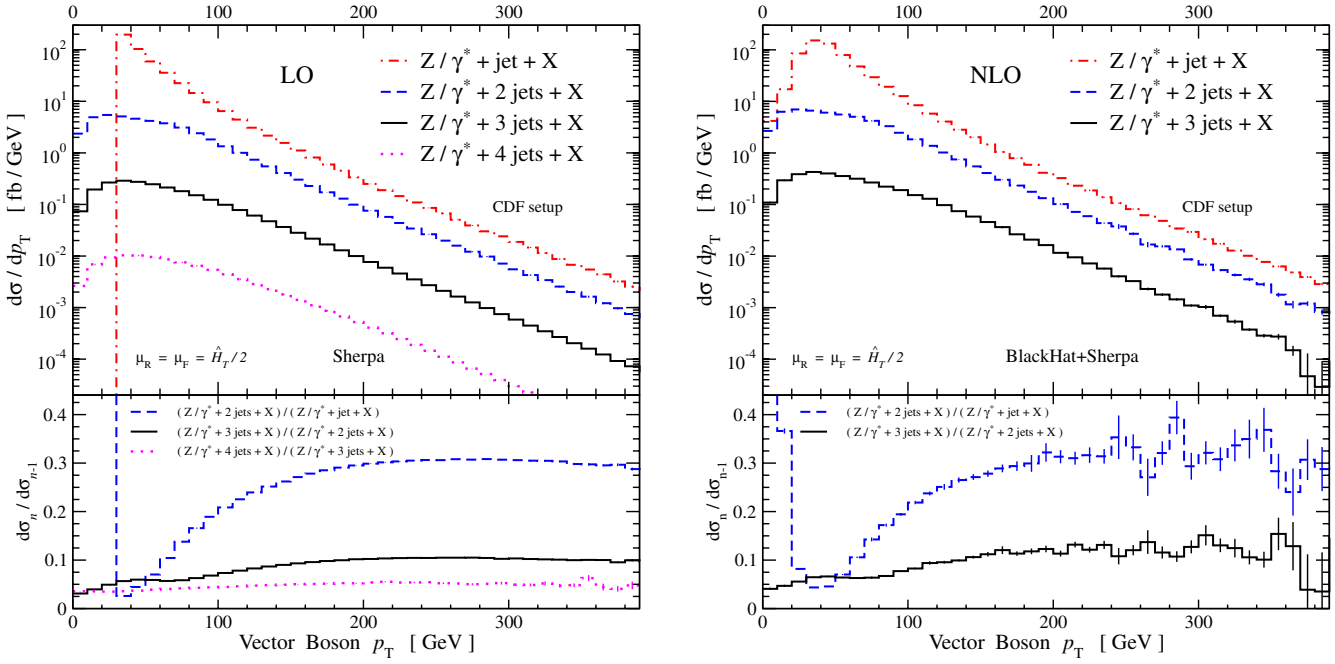

FIG. 15 (color online). The LO and NLO vector-boson p_T distributions for $Z,\gamma^* + n$-jet production at CDF. In the upper panels, the top distribution is for one-jet inclusive production, the one underneath it is for two-jet inclusive production, and the next one is for three-jet inclusive production. At LO, in the left plot the bottom curve is for four-jet production. The lower panel gives the jet-production ratios as a function of vector-boson p_T. In the bottom panel the upper curve is the 2/1-jet ratio and the one underneath it the 3/2-jet ratio. The 4/3-jet ratio at LO is displayed as well (magenta dotted curve).

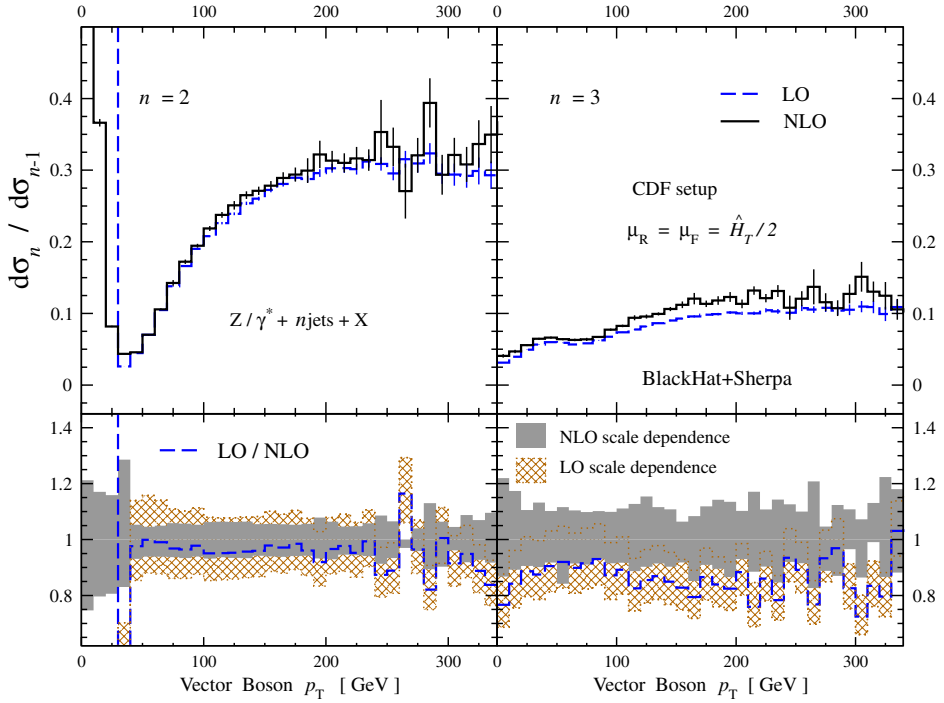

FIG. 16 (color online). Comparison of jet-production ratios, differential in the vector-boson p_T, at LO and NLO. The lower panel shows these ratios, divided by the NLO ratio evaluated at the default central scale choice, and including scale variation bands (computed as for the total cross-section ratios).

The behavior of the ratios at low p_T is relatively easy to understand. For p_T^V below the minimal jet p_T, the vector's transverse momentum cannot be balanced by a lone parton, so the leading-order contribution to $Z,\gamma^* + 1$-jet production vanishes. Accordingly, the $2/1$ ratio is infinite at LO for $p_T^V < p_{T\,\mathrm{min}}^{\mathrm{jet}}$, and rises from a very small value just above $p_T^V = p_{T\,\mathrm{min}}^{\mathrm{jet}}$. For $Z,\gamma^* + 1$-jet production at NLO, as $p_T^V \to 0$, the only contribution is from real-emission configurations with two partons which are roughly balanced in transverse momentum. It is reasonably likely that the second-hardest parton also has $p_T > p_{T\,\mathrm{min}}^{\mathrm{jet}}$. Therefore the differential cross section in this region is of the same order in α_s, $\mathcal{O}(\alpha_s^2)$, as the leading contribution to $Z,\gamma^* + 2$-jet production. Hence the NLO $2/1$ ratio rises as $p_T^V \to 0$, to a number independent of α_s (and "of order unity"). No such kinematic constraints arise in vector-boson production accompanied by more than one jet, even at LO, so the $3/2$ and $4/3$ ratios remain small as $p_T^V \to 0$.

What about the rise at larger vector-boson transverse momentum? For a given large p_T^V, we expect that the matrix element is maximized for an asymmetric configuration of jets, corresponding to a near-singular configuration of the partons. A typical configuration, for example, would have one hard jet recoiling against the vector, and additional jets (if any) with transverse momenta down near the p_T cut. In these configurations, the short-distance matrix element will factorize into a matrix element for production of one hard gluon, and a singular factor: either a splitting function in collinear limits, or an eikonal one in soft limits. The phase-space integrals over these near-singular configurations give rise to potentially large logarithms. Because the minimum ΔR is relatively large, collinear logarithms should not play an important role; on the other hand, $p_T^V/p_{T\,\mathrm{min}}^{\mathrm{jet}}$ can become large, so its logarithm will play a role.

The approximate factorization suggests that we can model the differential cross sections shown in Fig. 15 by the following forms:

$$\begin{aligned}
\sigma_1 &= a_s f(p_T^V), \\
\sigma_2 &= a_s^2(b_0 + b_1 \ln\rho) f(p_T^V)(1 - p_T^V/p_T^{\mathrm{max}})^{\gamma_2}, \\
\sigma_3 &= a_s^3(c_0 + c_1 \ln\rho + c_2 \ln^2\rho) f(p_T^V)(1 - p_T^V/p_T^{\mathrm{max}})^{\gamma_3}, \\
\sigma_4 &= a_s^4(d_0 + d_1 \ln\rho + d_2 \ln^2\rho + d_3 \ln^3\rho) \\
&\quad \times f(p_T^V)(1 - p_T^V/p_T^{\mathrm{max}})^{\gamma_4},
\end{aligned} \tag{6.1}$$

where $a_s \equiv \alpha_s(p_T^V) N_c/(2\pi)$, $\rho \equiv (p_T^V/p_{T\,\mathrm{min}}^{\mathrm{jet}})^2$, and $p_T^{\mathrm{max}} = 980$ GeV. The additional factors of $(1 - p_T^V/p_T^{\mathrm{max}})^{\gamma}$ take into account the limits of the different-dimension phase spaces and possibly different parton-distribution-function suppression in the four cases. The function $f(p_T^V)$, which describes the overall rapidly falling form of the distribution, will cancel in the ratios, leaving us with three parameters for the $2/1$ ratio, four additional

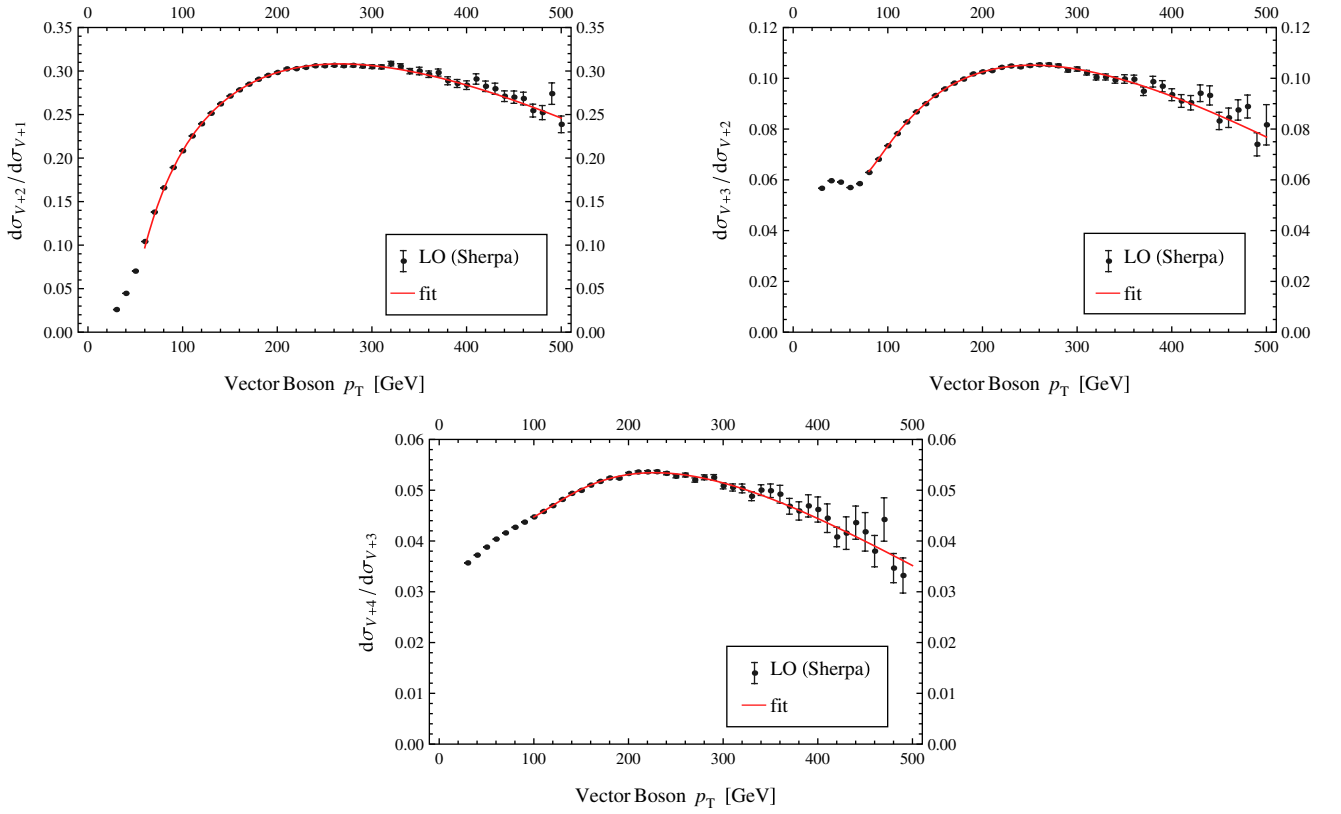

FIG. 17 (color online). Fits of the LO jet-production ratios (using CDF cuts) as a function of p_T to forms derived from Eq. (6.1). Top left, the $2/1$ ratio; top right, the $3/2$ ratio; bottom, the $4/3$ ratio. The vertical scales are different.

ones for the $3/2$ ratio, and five further parameters for the $4/3$ ratio.

We can determine these parameters for the CDF cuts by fitting the ratios to our LO results (where much smaller statistical uncertainties are easier to achieve). We evaluate the LO distributions at the central μ value, and fit in the range 100 GeV $\leq p_T^V \leq$ 500 GeV. The result is

$$\begin{aligned} &b_0 = -1.642, \quad b_1 = 2.437, \quad \gamma_2 = 1.118, \\ &c_0 = 5.081, \quad c_1 = -5.812, \quad c_2 = 2.658, \quad \gamma_3 = 2.539, \\ &d_0 = -5.728, \quad d_1 = 10.945, \quad d_2 = -6.4, \quad d_3 = 1.628, \quad \gamma_4 = 4.195. \end{aligned} \tag{6.2}$$

The separate fits to the LO ratios are shown in Fig. 17. In spite of the limited number of parameters, the model gives an excellent approximation to the LO ratios, even down to p_T^V of 70 GeV for the $2/1$ ratio. (For the $2/1$ ratio, the model's predictions are within 0.7% of the numerical results for two-thirds of the points in the fit range, and all points are within twice the Monte Carlo statistical error. For the $3/2$ ratio, two-thirds of the points in the fit range are within 1%.) Although we did not attempt a fit to the NLO results for the $2/1$ or $3/2$ ratios, due to larger statistical uncertainties, Fig. 16 indicates that the parameters entering the $2/1$ ratio would be essentially unchanged, and the $3/2$ ratio parameters would only change modestly. We stress that the model is a purely phenomenological one, with some physically motivated input as to its form. It is not intended to supply a perfect fit, but it is remarkable that it does so well with so few parameters.

The overall conclusion of this section is that the jet-production ratio is *not* solely a measure of α_s, but also depends sensitively on kinematical ratios.

VII. CONCLUSIONS

In this paper we have presented the first full NLO results for $Z,\gamma^* + 3$-jet production at a hadron collider. (Reference [48] contains a preliminary version of some of these results, based on a leading-color approximation.) We chose to present results for the Tevatron, so that we could compare to existing data from CDF and D0 [2,4]. Our study should also serve as a benchmark for future NLO

studies of Z-boson production in association with multiple jets at the LHC.

In line with expectations, we found that NLO results for $Z,\gamma^* + 1$, 2, 3-jet production are much less sensitive than their LO counterparts to the choice of a common renormalization and factorization scale μ. The deviation in the cross section, when varying μ around our default central scale choice by a factor of 2, drops from 60% at LO to 15%–22% at NLO. As noted in earlier studies [18,51], the commonly used scale choice of the vector-boson transverse energy is not particularly good at LHC energies, as it leads to large shape changes in distributions between LO and NLO. At LHC energies, this choice can even lead to negative cross sections at NLO, in tails of various distributions [18]. As we have shown in the present paper, this choice is also a poor one for higher-multiplicity $Z,\gamma^* + n$-jet production, even at Tevatron energies, because it generically results in large shape changes from LO to NLO. We used half the total transverse energy, $\mu = \hat{H}_T/2$, as our default scale choice instead.

The NLO results presented in this paper are parton-level results. To compare to the measurements, nonperturbative corrections need to be taken into account. We used the nonperturbative corrections tabulated by CDF and D0 to estimate the corrections to our parton-level predictions. These corrections were computed for different cone algorithms, and in the case of D0 selection (b), for a slightly different setup. We appealed to inclusive-jet studies [53,60] of algorithm differences to suggest that applying these corrections is reasonable; clearly, further study of this issue is desirable. Applying the corrections, we found good agreement between the NLO results and the CDF and D0 measurements of cross sections and jet p_T distributions. For $Z,\gamma^* + 3$-jet production, both CDF and D0 data lie somewhat higher than the theoretical scale-dependence band, although the statistical uncertainties are still large. Obviously, from the perspective of comparing to NLO results, it is helpful to choose infrared-safe jet algorithms, as well as cone sizes for which the nonperturbative corrections and their associated uncertainties are small.

For the cuts used by CDF, we presented results for two algorithms, SISCone and anti-k_T. The differences in cross sections for the two algorithms can be explained qualitatively by the larger effective cone size of SISCone [52,56,71], for a given cone-size parameter R.

We presented new results on jet-production ratios. We confirmed that for total cross sections the ratio of n-jet production to $(n-1)$-jet production is roughly constant [61,62]. For the cuts used by CDF, the NLO prediction gives ratios for $n = 2$, 3 that are within about 30% of each other, whereas for the cuts used by D0 the corresponding ratios are within about 15%. (We note that the ratios for D0's setup are about 50% higher than for CDF's setup.) In both cases, the NLO corrections to the LO ratios are quite small, 12% or less. This suggests that the LO prediction of the ratio should also be fairly reliable for $n = 4$, though confirmation awaits an NLO computation. In this case, however, the predicted ratio for $n = 4$ would lie significantly below the ratios for $n = 2$, 3. We expect that nonperturbative effects will partly cancel in the ratios, making them theoretically more robust. Although the jet-production ratios can be used to give a rough estimate of higher-multiplicity jet total cross sections, for differential cross sections there is a strong dependence on the cuts and the number of jets. In particular, we found that the ratios depend strongly on the vector-boson p_T. These ratios of distributions have generic features which we described using a simple model capturing leading logarithms along with phase-space and parton-distribution-function suppression factors. The fits based on this model are surprisingly good and offer a simple parametrization of the theoretical predictions.

Eventually, we would like to match the NLO results to parton showers and hadronization models, allowing nonperturbative effects to be modeled directly in an NLO program, instead of relying on LO-based tools to model them. This has been done for a variety of processes within the MC@NLO program [79] and the POWHEG method [80]. It would be desirable to extend this matching to higher-multiplicity processes such as those presented here. A first step in this direction, linking BLACKHAT to an automated implementation of the FKS subtraction formalism [44] used in MC@NLO, has been reported recently [15,81].

With the on-shell methods as implemented in BLACKHAT, we expect the computation of virtual corrections to cease presenting a bottleneck to obtaining new NLO results. A publicly available version of BLACKHAT is in preparation and is currently being tested in a variety of projects (see e.g. Ref. [81]). This version uses the proposed Binoth Les Houches interface for one-loop matrix elements [82]. It has been tested with both C++ and FORTRAN clients. We intend the public version to provide all processes that have been carefully tested with the full BLACKHAT code. The dipole-subtraction implementation that we used is available in the latest release of SHERPA [83].

NLO results will provide unprecedented precision for studies of vector bosons in association with many jets. They should prove useful for experimentally driven determinations of backgrounds such as the invisible $Z \to \nu\bar{\nu}$ background to missing-energy-plus-jets signatures. By measuring the corresponding $Z \to l^+l^-$ or $W \to l\nu$ processes, with NLO predictions for cross-section ratios providing the necessary conversion factors, the $Z \to \nu\bar{\nu}$ background can be determined precisely [19,20]. The results presented in this paper are examples of the predictions that can be obtained using BLACKHAT in conjunction with SHERPA. We look forward to applying these tools to a wide range of studies of the forthcoming LHC data.

ACKNOWLEDGMENTS

We thank Joey Huston, Sabine Lammers, Michael Peskin, Gavin Salam, Peter Skands, and Rainer Wallny for helpful conversations, and, in particular, Henrik Nilsen for useful discussions and comments on the manuscript. This research was supported by the U.S. Department of Energy under Contracts No. DE-FG03-91ER40662, No. DE-AC02-76SF00515, and No. DE-FC02-94ER40818. D. A. K.'s research was supported by the European Research Council under the Advanced Investigator Grant No. ERC-AdG-228301. H. I.'s work was supported by a grant from the U.S. LHC Theory Initiative through NSF Contract No. PHY-0705682. This research used resources of Academic Technology Services at UCLA, PhenoGrid using the GridPP infrastructure, and the National Energy Research Scientific Computing Center, which is supported by the Office of Science of the U.S. Department of Energy under Contract No. DE-AC02-05CH11231.

APPENDIX A: KINEMATICS AND OBSERVABLES

In this Appendix we give our definitions of standard kinematic variables used to characterize scattering events. The angular separation of two objects (partons, jets, or leptons) is denoted by

$$\Delta R = \sqrt{(\Delta\phi)^2 + (\Delta y)^2}, \tag{A1}$$

with $\Delta\phi$ the difference in the azimuthal angles, and Δy the difference in the rapidities. The rapidity is defined to be

$$y = \frac{1}{2}\ln\left(\frac{E + p_L}{E - p_L}\right), \tag{A2}$$

where E is the energy and p_L is the component of the momentum along the beam axis (the z axis). The pseudorapidity η is given by

$$\eta = -\ln\left(\tan\frac{\theta}{2}\right) = \frac{1}{2}\ln\left(\frac{|\vec{p}| + p_L}{|\vec{p}| - p_L}\right), \tag{A3}$$

where θ is the polar angle with respect to the beam axis.

Jets are formed using cluster or cone algorithms based on the angular separation (A1). It is also possible to use the pseudorapidity in place of the rapidity. We have checked, for the production of $Z,\gamma^* + 3$ jets at NLO, that using η instead of y for the anti-k_T and k_T algorithms with $R = 0.5$ makes no discernible difference on the cross section.

The transverse energies of massless outgoing partons and leptons, $E_T = \sqrt{p_x^2 + p_y^2}$, can be summed to give the total partonic transverse energy, $\hat{H}_T$, of the scattering process,

$$\hat{H}_T = \sum_p E_T^p + E_T^{e^+} + E_T^{e^-}. \tag{A4}$$

All final-state partons p and leptons are included in $\hat{H}_T$, whether or not they are inside jets that pass the cuts. As discussed in Sec. III D, the variable $\hat{H}_T$ represents a good choice for the renormalization and factorization scale of a given event. Although the partonic version is not directly measurable, for practical purposes as a scale choice, it is essentially equivalent (and identical at LO) to the more usual jet-based total transverse energy,

$$H_T = \sum_j E_{T,j}^{\text{jet}} + E_T^{e^+} + E_T^{e^-}. \tag{A5}$$

The jet four-momenta are computed by summing the four-momenta of all partons that are clustered into them,

$$p_\mu^{\text{jet}} = \sum_{i\in\text{jet}} p_{i\mu}. \tag{A6}$$

The jet transverse momentum is then defined in the usual way,

$$p_T^{\text{jet}} = \sqrt{(p_x^{\text{jet}})^2 + (p_y^{\text{jet}})^2}. \tag{A7}$$

APPENDIX B: SQUARED MATRIX ELEMENTS AT ONE POINT IN PHASE SPACE

As an aid to future implementation of $Z,\gamma^* + 3$-jet production in other numerical codes, we present values of the one-loop virtual corrections to the squared matrix elements, $d\sigma_V^{(1)}$, at one point in phase space. These contributions arise from the interference between the tree and one-loop amplitudes, summed over all colors and helicities, for $N_c = 3$ and $n_f = 5$ massless quark flavors. As discussed in the text, we do not include the small effects

TABLE IX. Numerical values of the normalized virtual correction to the squared matrix elements, $\widehat{d\sigma_V^{(1)}}$, at the phase-space point given in Eq. (B3), for three basic partonic subprocesses for $Z + 3$-jet production at a hadron collider. We give both the finite parts and the coefficients of the poles in ϵ.

$\widehat{d\sigma_V^{(1)}}$	$1/\epsilon^2$	$1/\epsilon$	ϵ^0
$(1_{\bar{u}}2_d \to 3_d4_{\bar{u}}5_g6_{e^-}7_{e^+})$	−8.333 333 333 3	−32.374 560 649 5	5.237 471 627 7
$(1_{\bar{u}}2_u \to 3_u4_{\bar{u}}5_g6_{e^-}7_{e^+})$	−8.333 333 333 3	−32.518 090 299 8	0.438 741 299 4
$(1_{\bar{u}}2_g \to 3_g4_g5_{\bar{u}}6_{e^-}7_{e^+})$	−11.666 666 666 7	−42.327 926 651 8	−15.232 608 285 3

from the top quark, or from axial or vectorial loop contributions (see Fig. 2).

In Table IX we present numerical values for three representative subprocesses. The other subprocesses are related to these by crossing symmetry or by change of coupling constants. In the second line of Table IX, the presence of two identical quarks (after crossing all particles into the final state) implies that amplitudes are antisymmetrized under exchange of the two.

We quote numerical results for the ultraviolet-renormalized virtual corrections in the 't Hooft–Veltman variant of dimensional regularization [84]. The remaining singularities in the dimensional regularization parameter $\epsilon = (4 - D)/2$ arise from the virtual soft and collinear singularities in the one-loop amplitudes.

The quoted values are for the ratio of the virtual corrections to the tree-level squared matrix element $d\sigma^{(0)}$. Explicitly, we define the ratio,

$$\widehat{d\sigma}_V^{(1)} \equiv \frac{1}{8\pi\alpha_S c_\Gamma(\epsilon)} \frac{d\sigma_V^{(1)}}{d\sigma^{(0)}}, \tag{B1}$$

where we have also separated out the dependence on the strong coupling α_S and the overall factor $c_\Gamma(\epsilon)$, defined by

$$c_\Gamma(\epsilon) = \frac{1}{(4\pi)^{2-\epsilon}} \frac{\Gamma(1+\epsilon)\Gamma^2(1-\epsilon)}{\Gamma(1-2\epsilon)}. \tag{B2}$$

The coupling constants, mass, and width of the Z boson are given in Sec. III A.

We choose the phase-space point given in Eqs. (9.3) and (9.4) of Ref. [25],

$$\begin{aligned}
k_1 &= \frac{\mu}{2}(1, -\sin\theta, -\cos\theta\sin\phi, -\cos\theta\cos\phi),\\
k_2 &= \frac{\mu}{2}(1, \sin\theta, \cos\theta\sin\phi, \cos\theta\cos\phi),\\
k_3 &= \frac{\mu}{3}(1, 1, 0, 0), \qquad k_4 = \frac{\mu}{8}(1, \cos\beta, \sin\beta, 0),\\
k_5 &= \frac{\mu}{10}(1, \cos\alpha\cos\beta, \cos\alpha\sin\beta, \sin\alpha),\\
k_6 &= \frac{\mu}{12}(1, \cos\gamma\cos\beta, \cos\gamma\sin\beta, \sin\gamma),\\
k_7 &= k_1 + k_2 - k_3 - k_4 - k_5 - k_6,
\end{aligned} \tag{B3}$$

where

$$\begin{aligned}
\theta &= \frac{\pi}{4}, \qquad \phi = \frac{\pi}{6}, \qquad \alpha = \frac{\pi}{3},\\
\gamma &= \frac{2\pi}{3}, \qquad \cos\beta = -\frac{37}{128},
\end{aligned} \tag{B4}$$

and the renormalization scale μ_R is set to $\mu_R = 7$ GeV. We have flipped the signs of k_1 and k_2 compared to Ref. [25], to correspond to $2 \to 5$ kinematics, instead of $0 \to 7$ kinematics. The labeling of the parton and lepton momenta is indicated explicitly in the first column of Table IX.

[1] S. D. Ellis, R. Kleiss, and W. J. Stirling, Phys. Lett. **158B**, 341 (1985); M. L. Mangano, Eur. Phys. J. C **59**, 373 (2009).

[2] T. Aaltonen *et al.* (CDF Collaboration), Phys. Rev. Lett. **100**, 102001 (2008).

[3] V. M. Abazov *et al.* (D0 Collaboration), Phys. Lett. B **669**, 278 (2008).

[4] V. M. Abazov *et al.* (D0 Collaboration), Phys. Lett. B **678**, 45 (2009).

[5] V. M. Abazov *et al.* (D0 Collaboration), Phys. Lett. B **682**, 370 (2010).

[6] T. Stelzer and W. F. Long, Comput. Phys. Commun. **81**, 357 (1994); A. Pukhov *et al.*, arXiv:hep-ph/9908288; M. L. Mangano, M. Moretti, F. Piccinini, R. Pittau, and A. D. Polosa, J. High Energy Phys. 07 (2003) 001.

[7] A. Kanaki and C. G. Papadopoulos, Comput. Phys. Commun. **132**, 306 (2000).

[8] F. Krauss, R. Kuhn, and G. Soff, J. High Energy Phys. 02 (2002) 044.

[9] S. Catani, F. Krauss, R. Kuhn, and B. R. Webber, J. High Energy Phys. 11 (2001) 063; M. Mangano, Fermilab ME/MC TuningWorkshop.

[10] M. L. Mangano, M. Moretti, F. Piccinini, and M. Treccani, J. High Energy Phys. 01 (2007) 013; S. Mrenna and P. Richardson, J. High Energy Phys. 05 (2004) 040.

[11] H. U. Bengtsson and T. Sjöstrand, Comput. Phys. Commun. **46**, 43 (1987); T. Sjöstrand, P. Eden, C. Friberg, L. Lönnblad, G. Miu, S. Mrenna, and E. Norrbin, Comput. Phys. Commun. **135**, 238 (2001); T. Sjöstrand, L. Lönnblad, S. Mrenna, and P. Skands, arXiv:hep-ph/0308153; T. Sjöstrand, S. Mrenna, and P. Z. Skands, J. High Energy Phys. 05 (2006) 026.

[12] G. Marchesini and B. R. Webber, Nucl. Phys. **B310**, 461 (1988); G. Marchesini, B. R. Webber, G. Abbiendi, I. G. Knowles, M. H. Seymour, and L. Stanco, Comput. Phys. Commun. **67**, 465 (1992); G. Corcella *et al.*, arXiv:hep-ph/0210213; M. Bähr *et al.*, Eur. Phys. J. C **58**, 639 (2008).

[13] T. Gleisberg, S. Höche, F. Krauss, M. Schönherr, S. Schumann, F. Siegert, and J. Winter, J. High Energy Phys. 02 (2009) 007.

[14] Z. Bern *et al.*, arXiv:0803.0494.

[15] T. Binoth *et al.*, arXiv:1003.1241.

[16] T. Aaltonen *et al.* (CDF Collaboration), Phys. Rev. D **77**, 011108 (2008).

[17] C. F. Berger *et al.*, Phys. Rev. Lett. **102**, 222001 (2009).
[18] C. F. Berger *et al.*, Phys. Rev. D **80**, 074036 (2009).
[19] CMS Collaboration, http://cdsweb.cern.ch/record/1194471/files/SUS-08-002-pas.pdf.
[20] G. Aad *et al.* (ATLAS Collaboration), arXiv:0901.0512, p. 1552.
[21] Z. Bern, L. J. Dixon, D. C. Dunbar, and D. A. Kosower, Nucl. Phys. **B425**, 217 (1994); **B435**, 59 (1995); Z. Bern, L. J. Dixon, and D. A. Kosower, Annu. Rev. Nucl. Part. Sci. **46**, 109 (1996).
[22] Z. Bern, L. J. Dixon, and D. A. Kosower, Nucl. Phys. **B513**, 3 (1998).
[23] R. Britto, F. Cachazo, and B. Feng, Nucl. Phys. **B725**, 275 (2005).
[24] R. Britto, F. Cachazo, B. Feng, and E. Witten, Phys. Rev. Lett. **94**, 181602 (2005); Z. Bern, L. J. Dixon, and D. A. Kosower, Phys. Rev. D **71**, 105013 (2005); **72**, 125003 (2005); **73**, 065013 (2006); D. Forde and D. A. Kosower, Phys. Rev. D **73**, 065007 (2006); **73**, 061701 (2006); C. F. Berger, Z. Bern, L. J. Dixon, D. Forde, and D. A. Kosower, Phys. Rev. D **75**, 016006 (2007).
[25] C. F. Berger, Z. Bern, L. J. Dixon, D. Forde, and D. A. Kosower, Phys. Rev. D **74**, 036009 (2006).
[26] G. Ossola, C. G. Papadopoulos, and R. Pittau, Nucl. Phys. **B763**, 147 (2007).
[27] D. Forde, Phys. Rev. D **75**, 125019 (2007).
[28] R. K. Ellis, W. T. Giele, and Z. Kunszt, J. High Energy Phys. 03 (2008) 003.
[29] W. T. Giele, Z. Kunszt, and K. Melnikov, J. High Energy Phys. 04 (2008) 049.
[30] Z. Bern, L. J. Dixon, and D. A. Kosower, Ann. Phys. (N.Y.) **322**, 1587 (2007); C. F. Berger and D. Forde, arXiv:0912.3534.
[31] C. F. Berger, Z. Bern, L. J. Dixon, F. Febres Cordero, D. Forde, H. Ita, D. A. Kosower, and D. Maître, Phys. Rev. D **78**, 036003 (2008).
[32] C. F. Berger, Z. Bern, L. J. Dixon, F. Febres Cordero, D. Forde, H. Ita, D. A. Kosower, and D. Maître, arXiv:0808.0941.
[33] G. Ossola, C. G. Papadopoulos, and R. Pittau, J. High Energy Phys. 03 (2008) 042; W. T. Giele and G. Zanderighi, J. High Energy Phys. 06 (2008) 038; A. Lazopoulos, arXiv:0812.2998; J.-C. Winter and W. T. Giele, arXiv:0902.0094.
[34] A. van Hameren, C. G. Papadopoulos, and R. Pittau, J. High Energy Phys. 09 (2009) 106.
[35] R. K. Ellis, W. T. Giele, Z. Kunszt, K. Melnikov, and G. Zanderighi, J. High Energy Phys. 01 (2009) 012.
[36] R. K. Ellis, K. Melnikov, and G. Zanderighi, J. High Energy Phys. 04 (2009) 077; Phys. Rev. D **80**, 094002 (2009); K. Melnikov and G. Zanderighi, Phys. Rev. D **81**, 074025 (2010).
[37] G. Bevilacqua, M. Czakon, C. G. Papadopoulos, R. Pittau, and M. Worek, J. High Energy Phys. 09 (2009) 109.
[38] A. Bredenstein, A. Denner, S. Dittmaier, and S. Pozzorini, J. High Energy Phys. 08 (2008) 108; Phys. Rev. Lett. **103**, 012002 (2009); J. High Energy Phys. 03 (2010) 021.
[39] T. Binoth, N. Greiner, A. Guffanti, J. P. Guillet, T. Reiter, and J. Reuter, Phys. Lett. B **685**, 293 (2010).
[40] G. Bevilacqua, M. Czakon, C. G. Papadopoulos, and M. Worek, Phys. Rev. Lett. **104**, 162002 (2010).
[41] J. M. Campbell and R. K. Ellis, Phys. Rev. D **65**, 113007 (2002).
[42] S. Catani and M. H. Seymour, Phys. Lett. B **378**, 287 (1996); Nucl. Phys. **B485**, 291 (1997); **B510**, 503(E) (1998).
[43] T. Gleisberg and F. Krauss, Eur. Phys. J. C **53**, 501 (2008).
[44] S. Frixione, Z. Kunszt, and A. Signer, Nucl. Phys. **B467**, 399 (1996).
[45] M. H. Seymour and C. Tevlin, arXiv:0803.2231; K. Hasegawa, S. Moch, and P. Uwer, Nucl. Phys. B, Proc. Suppl. **183**, 268 (2008); R. Frederix, T. Gehrmann, and N. Greiner, J. High Energy Phys. 09 (2008) 122; M. Czakon, C. G. Papadopoulos, and M. Worek, J. High Energy Phys. 08 (2009) 085; R. Frederix, S. Frixione, F. Maltoni, and T. Stelzer, J. High Energy Phys. 10 (2009) 003.
[46] A. van Hameren and C. G. Papadopoulos, Eur. Phys. J. C **25**, 563 (2002).
[47] T. Gleisberg, S. Höche, and F. Krauss, arXiv:0808.3672.
[48] C. F. Berger *et al.*, Proc. Sci., RADCOR2009 (2009) 065.
[49] S. Frixione, Nucl. Phys. **B410**, 280 (1993); U. Baur, T. Han, and J. Ohnemus, Phys. Rev. D **53**, 1098 (1996); **57**, 2823 (1998); L. J. Dixon, Z. Kunszt, and A. Signer, Phys. Rev. D **60**, 114037 (1999); G. Bozzi, B. Jäger, C. Oleari, and D. Zeppenfeld, Phys. Rev. D **75**, 073004 (2007).
[50] M. L. Mangano and S. J. Parke, Phys. Rev. D **41**, 59 (1990).
[51] C. W. Bauer and B. O. Lange, arXiv:0905.4739.
[52] G. P. Salam, Eur. Phys. J. C **67**, 637 (2010).
[53] G. P. Salam and G. Soyez, J. High Energy Phys. 05 (2007) 086.
[54] M. Cacciari, G. P. Salam, and G. Soyez, J. High Energy Phys. 04 (2008) 063.
[55] S. Catani, Y. L. Dokshitzer, M. H. Seymour, and B. R. Webber, Nucl. Phys. **B406**, 187 (1993).
[56] S. D. Ellis and D. E. Soper, Phys. Rev. D **48**, 3160 (1993).
[57] R. Akers *et al.* (OPAL Collaboration), Z. Phys. C **63**, 197 (1994); M. H. Seymour, Nucl. Phys. **B513**, 269 (1998).
[58] G. C. Blazey *et al.*, in *Proceedings of the Workshop: QCD and Weak Boson Physics in Run II*, edited by U. Baur, R. K. Ellis, and D. Zeppenfeld (Fermilab-Pub-00/297, 2000).
[59] A. Abulencia *et al.* (CDF Collaboration), Phys. Rev. D **74**, 071103(R) (2006).
[60] S. D. Ellis, J. Huston, K. Hatakeyama, P. Loch, and M. Tonnesmann, Prog. Part. Nucl. Phys. **60**, 484 (2008).
[61] S. D. Ellis, R. Kleiss, and W. J. Stirling, Phys. Lett. **154B**, 435 (1985); F. A. Berends, W. T. Giele, H. Kuijf, R. Kleiss, and W. J. Stirling, Phys. Lett. B **224**, 237 (1989); F. A. Berends, H. Kuijf, B. Tausk, and W. T. Giele, Nucl. Phys. **B357**, 32 (1991).
[62] E. Abouzaid and H. J. Frisch, Phys. Rev. D **68**, 033014 (2003).
[63] G. 't Hooft and M. J. G. Veltman, Nucl. Phys. **B153**, 365 (1979); G. J. van Oldenborgh and J. A. M. Vermaseren, Z. Phys. C **46**, 425 (1990); W. Beenakker and A. Denner, Nucl. Phys. **B338**, 349 (1990); A. Denner, U. Nierste, and R. Scharf, Nucl. Phys. **B367**, 637 (1991); Z. Bern, L. J. Dixon, and D. A. Kosower, Nucl. Phys. **B412**, 751 (1994); T. Hahn and M. Pérez-Victoria, Comput. Phys. Commun.

118, 153 (1999); R. K. Ellis and G. Zanderighi, J. High Energy Phys. 02 (2008) 002.
[64] S. D. Badger, J. High Energy Phys. 01 (2009) 049.
[65] Z. Bern and A. G. Morgan, Nucl. Phys. **B467**, 479 (1996); Z. Bern, L. J. Dixon, D. C. Dunbar, and D. A. Kosower, Phys. Lett. B **394**, 105 (1997); C. Anastasiou, R. Britto, B. Feng, Z. Kunszt, and P. Mastrolia, Phys. Lett. B **645**, 213 (2007); R. Britto and B. Feng, J. High Energy Phys. 02 (2008) 095.
[66] Z. Bern, L. J. Dixon, and D. A. Kosower, Nucl. Phys. **B437**, 259 (1995).
[67] W. Giele, Z. Kunszt, and J. Winter, arXiv:0911.1962.
[68] Y. Hida, X. S. Li, and D. H. Bailey, Report No. LBNL-46996 [http://crd.lbl.gov/~dhbailey/mpdist].
[69] R. Kleiss and R. Pittau, Comput. Phys. Commun. **83**, 141 (1994).
[70] J. Pumplin *et al.*, J. High Energy Phys. 07 (2002) 012.
[71] M. Dasgupta, L. Magnea, and G. P. Salam, J. High Energy Phys. 02 (2008) 055.
[72] J. Huston, Proc. Sci., RADCOR2009 (2010) 079.
[73] D. de Florian and W. Vogelsang, Phys. Rev. D **76**, 074031 (2007).
[74] M. Rubin, G. P. Salam, and S. Sapeta, arXiv:1006.2144.
[75] F. Abe *et al.* (CDF Collaboration), Phys. Rev. D **45**, 1448 (1992).
[76] R. K. Ellis, W. J. Stirling, and B. R. Webber, *QCD and Collider Physics* (Cambridge University Press, Cambridge, England, 1996).
[77] C. Anastasiou, L. J. Dixon, K. Melnikov, and F. Petriello, Phys. Rev. D **69**, 094008 (2004).
[78] V. M. Abazov *et al.* (D0 Collaboration), Phys. Rev. D **67**, 012004 (2003); W. Wagner *et al.* (CDF Collaboration), Eur. Phys. J. C **33**, s238 (2004); D. Cho, Ph.D. thesis, Fermilab 2005-31 [UMI-31-69569-MC] [http://lss.fnal.gov/archive/thesis/index.shtml].
[79] S. Frixione and B. R. Webber, J. High Energy Phys. 06 (2002) 029; S. Frixione, P. Nason, and B. R. Webber, J. High Energy Phys. 08 (2003) 007.
[80] P. Nason, J. High Energy Phys. 11 (2004) 040; S. Frixione, P. Nason, and C. Oleari, J. High Energy Phys. 11 (2007) 070; S. Alioli, P. Nason, C. Oleari, and E. Re, J. High Energy Phys. 07 (2008) 060; 06 (2010) 043.
[81] R. Frederix, Proc. Sci., RADCOR2009 (2009) 066.
[82] T. Binoth *et al.*, Comput. Phys. Commun. **181**, 1612 (2010).
[83] SHERPA home page, http://www.sherpa-mc.de/.
[84] G. 't Hooft and M. Veltman, Nucl. Phys. **B44**, 189 (1972).